NASA TECHNICAL MEMORANDUM NASA TM-75840

DEVELOPMENT AND WIND TUNNEL INVESTIGATION OF THREE SUPERCRITICAL AIRFOIL PROFILES FOR TRANSPORT AIRCRAFT

Translation of Entwicklung und Windkanalerprobung von drei ueberkritischen Tragfluegelprofilen fuer Verkehrsflugzeuge, Deutsche Gesellschaft fuer Luft-und Raumfahrt, Jahrestagung, 7th, Kiel, West Germany, Sept. 17-19, 1974, DGLR paper 74-100, 54 p.

NATIONAL AERONAUTICS AND SPACE ADMINISTRATION
WASHINGTON, D.C. 20546 NOVEMBER 1980

STANDARD TITLE PAGE

1. Report No. NASA TM-75840	2. Government Accession No.	3. Recipient's Catalog No.
4. Title and Subtitle DEVELOPMENT AND WIND TUNNEL INVESTIGATION OF THREE SUPERCRITICAL AIRFOIL PROFILES FOR TRANSPORT AIRCRAFT		5. Report Date November 1980 6. Performing Organization Code
7. Author(s) E. Stanewsky, H. Zimmer		8. Performing Organization Report No. 10. Work Unit No.
9. Performing Organization Name and Address SCITRAN Box 5456 Santa Barbara, CA 93108		11. Contract or Grant No. NASW-3198 13. Type of Report and Period Covered Translation
12. Sponsoring Agency Name and Address National Aeronautics and Space Administration Washington, D.C. 20546		14. Sponsoring Agency Code

15. Supplementary Notes
Translation of Entwicklung und Windkanalerprobung von drei ueberkritischen Tragfluegelprofilen fuer Verkehrsflugzeuge, Deutsche Gesellschaft fuer Luft-und Raumfahrt, Jahrestagung, 7th, Kiel, West Germany, Sept. 17-19, 1974, DGLR Paper 74-100, 54 p. (A75-24147)

16. Abstract
The present paper constitutes an abstract of a study concerned with the development of supercritical airfoils for transport aircraft which was carried out by DORNIER in cooperation with the DFVLR-(AVA) Goettingen. The first part of the paper describes the design cycle of the airfoils and their investigation in the wind tunnel, the second part is concerned with the effect of Reynolds number and the mode and location of transition on the transonic flow development.

17. Key Words (Selected by Author(s))	18. Distribution Statement		
	Unclassified - Unlimited		
19. Security Classif. (of this report) Unclassified	20. Security Classif. (of this page) Unclassified	21. No. of Pages 50	22.

NASA-HQ

DEVELOPMENT AND WIND TUNNEL INVESTIGATION OF THREE SUPER-CRITICAL AIR FLOWS FOR TRANSPORT AIRCRAFT*

/1#

E. Stanewsky, H. Zimmer**

*7th Annual Meeting of the DGLR (German Association for Aviation and Space Flight) Kiel, West Germany, September 17-19, 1974. Paper no. 74-100.

**German Association and Test Facility for Aerodynamics and Space Flight. Aerodynamic Test Facility, Goettingen, Dornier GmbH, Friedrichshafen, West Germany. Institute for Fluid Mechanics. September, 1974.

#Numbers in margin indicate pagination of foreign text.

+Some of the work of this paper was supported with BMFT funds. Contract No. 523-8891-LFF3.

Table of Contents /3

1. NOTATION

/4

a	speed of sound
C_A	lift coefficient
C_W	drag coefficient
$C_{m(25)}, C_m$	pitch moment coefficient (referred to the 1/4 line)
C_p	pressure coefficient $\frac{p - p_\infty}{q_\infty}$
C_p^+	pressure coefficient at $Ma_L = 1.0$
C_{pHK}	pressure coefficient at the profile trailing edge
H	tunnel height
J, J+1, J+2	net lines on the profile
K	transonic similarity parameter
l, c	profile chord
Ma	Mach number, V/a
Ma_L	local Mach number
n	arbitrary iteration step
p	static pressure (local)
p_∞	static pressure of incident flow
q_∞	stagnation pressure of incident flow $\rho/2 \cdot V^2$
Re	Reynolds number $\frac{\rho \cdot V \cdot l}{\mu}$
s, t	separations of net lines on the profile
V	incident speed
x/l, x/c	dimensionless x-coordinate of the profile
x_N/l	neutral point position
$(x/l)_{St}$	shock position
$\tilde{y}$	transformed ordinate
z/l	dimensionless profile thickness
α	geometric angle of attack
α_{korr}	corrected angle of attack (downwind correction)
γ_o	circulation
δ	maximum profile thickness
ρ	density
Φ	transonic perturbation potential
μ	dynamic viscosity
κ	ratio of specific heats ($\kappa = 1.4$)
ω_1, ω_2	relaxation factors

2. DEVELOPMENT AND TESTING OF SUPERCRITICAL PROFILES

/6

2.1 DIRECT-INVERSE METHOD FOR CALCULATING TRANSONIC PROFILE FLOW

Several design methods for transonic profiles are known. Several hodograph and relaxation methods [1] have become very important. Within the framework of this study, we developed an inverse relaxation method because it is simpler to operate in the physical plane than using the complex hodographs. Also it is impossible to generalize to the three-dimensional design case in a relatively simple manner.

2.1.1 The direct method (Figure 1)

The modified method of Murman, Cole, Krupp is used as the point of departure. Through partial linearization, introduction of a trial solution for the perturbation potential, matching of the introduced similarity parameter and the ordinate transformation we obtained the transonic potential equation for the perturbation potential Φ (Equation(1) from the exact potential equation. This is shown by Equation (1), Figure 1 which can be used for flows containing shocks. The solution of this mixed differential equation is done using the boundary condition on the profile according to Equation (2), conditions of infinity according to Equation (3) and the Kutta condition according to Equation (4). This is done numerically by transforming it into a difference equation.

For this purpose a network is placed over the flow field and for each node point we formulate a difference equation corresponding to each flow state. For each column we find a tridiagonal equation system which is closed by means of a boundary condition. Since the coefficients of this equation system depend on its solution, the solution is then iterated using a relaxation method. Iteration is performed until a certain column conversion criterion is satisfied. Then it advances to the next column until the entire field is covered.

The field must be analyzed by iteration until a certain convergence /7 criterion is satisfied. From the known potential distribution, we obtain the pressure distribution by means of numerical differentiation according to Equation (5). By integrating it over the profile we find the lift coefficient according to Equation (6).

2.1.2 The inverse method (Figure 2)

A successful way for the development of an inverse method was taken by Langley [1]. He starts with the fact that the flow has no vortices (Equation (7), Figure 2). By means of extrapolation and differentiation between two field iterations, $\Phi_{x\tilde{y}}$ over the profile we determine the pressure distribution according to Equation (8). The latter can also be used for a non-equidistant network, in contrast to Langley. The integration of $\Phi_{x\tilde{y}}$ over x according to Equation (9) results in $\Phi_{\tilde{y}}$ according to Equation (10). This new $\Phi_{\tilde{y}}$ is substituted into the direct method just as in the recalculation problem. In order to avoid jump changes, two relaxation factors are introduced. In addition, it is assumed that the profile nodes (up to 5% of the chord) are given. This restriction, however, is not very restrictive in practice.

2.2 The design cycle of supercritical profiles

Establishing this computation method is not enough for carrying out a profile design, because it is just as important to know the boundary layer as to know the external flow. The computation methods must be combined into a meaningful iteration cycle. The design cycle shown in Figure 3 applies if the direct method and the boundary layer method are available. This design cycle is based on the classical concept of the "profile plus displacement thickness". At the beginning we have the design requirements and the initial profile. During the design the aerodynamic and structural requirements are tested again and again until the requirements are met. In an internal loop, the contour has to be changed until the pressure /8

distribution meets the requirements. The first potential design was made according to this method. This rather difficult method is considerably facilitated by using the direct-inverse method, which was used for the other two profiles (Figure 4). The profile design, however, still remains a process which is too complicated so that it could be performed with simple computation. In addition, the profile is only as good as the weakest link in the transonic method-boundary method-wind tunnel chain.

2.3 Example of a transonic profile flow

From the following example we will clarify the influences mentioned. Figure 5 shows the profile end of the AIRBUS profile with the theoretical displacement thicknesses for two cases above the design Mach number Ma = 0.725. Since the wake flow of the profile influences the circulation, we can see from this figure that the boundary layer must have a great influence on the profile flow. Curve 1 in Figure 6 shows measurements and calculations without the influence of the boundary layer. As expected, there is a wide discrepancy. If we consider the influence of the displacement thickness we obtain the result shown in Curve 2 of Figure 6. If we consider the jet curvature correction of the corresponding wind tunnel, which depends on the lift coefficient and the Mach number, we obtain Curve 3 as a result, which agrees very well with measurements.

2.4 Design of airfoil profiles for commercial aircraft

In the commercial aircraft we are most interested in the most economic cruise condition. This depends greatly on the shape of the wing, and the base profile is very important. Figure 7 shows the required design point for the two-dimensional base profile. The /9
required lift coefficients depend on the sweep angle and the intended flight altitude at a given cruise Mach number. Here we will attempt to reach points as far to the right as possible using 12% thick profiles. The AIRBUS profile is used for comparison. Figure 8 shows

the most important design characteristics of the profiles developed here. The geometric shape of the profiles is shown in Figure 9.

With the first profile (CAST 7), the design specification is already satisfied. Also, the sweep of the AIRBUS can be reduced from 25° to 12°. Therefore, the second profile (CAST 10-2) was designed for the smallest possible pitch moment and the greatest thickness at the end of the profile in order to install a light flap system. A slight deterioration of the aerodynamic properties was acceptable. In the third profile (CAST 12-1) the highest design Mach number (Ma = 0.78) was desired. Pitch moment was not to be larger than that of profile CAST 7 and compared with it, we wish to achieve a structural improvement, that is, a thicker profile tip.

2.5 Wind tunnel testing of the designed profiles

The three profiles were tested in the 1 x 1 meter transonic wind tunnel of the DFVLR-(AVA) Goettingen [2-3] in a Mach number range between Ma = 0.50 and Ma = 0.90. Geometric angles of attack varied between $\alpha=-2°$ and $\alpha=9°$. The span of the model was B = 1000 mm and the profile chord was l = 200 mm. The Reynolds number referred to the wing chord was $Re = 2.4 \cdot 10^6$. The measurements for investigating profiles were carried out using a smooth model, that is a model without transition strips. The model is shown in Figure 10. Details about the test conditions and instrumentation of the model were given in [4]. The results are presented in [4] and [5]. Figure 11 shows /10 the measured and calculated pressure distribution of the various profiles at the theoretical design point as well as the theoretical transition point of the boundary layer. If we consider the fact that the measured operating points in general do not agree with the theoretical design point, we can say that this agreement is good in all three cases. Figure 12a to 12c show the pressure distributions of the profiles in the vicinity of the drag increase and the variations of the lift coefficient and the drag coefficient as a function of Mach number for the designed angle of attack.

Figure 13 can be used to find the moments of the various profiles for the cruise state. From Figure 14 we can find the neutral point positions. The profile CAST 10-2 has the smallest pitch moment so that if it is used, we can expect the smallest trim drag for it.

Figures 15 and 16 show the profile limit curves which are very important in practice. We can see the drag rise boundary from Figure 15 and the buffet boundary in Figure 16. In both cases, we see a sufficiently large lift reserve and Mach number reserve between the design requirements and the boundary curve. The improvement with respect to the AIRBUS profile is clear. However, we should consider the fact that this profile was measured under different conditions ($Re = 6 \cdot 10^6$, forced transition at 7%). In the second following part we will discuss the influence of the Reynolds number and transition.

3. INFLUENCE OF REYNOLDS NUMBER AND TRANSITION ON THE FLOW DEVELOPMENT AROUND SUPERCRITICAL PROFILES* /11

3.1 General remarks

For a long time it was believed that the influence of viscosity and, therefore, of Reynolds number was small in the transonic range. And then it was possible to determine the flow development of a full scale model if transition strips were applied to models to determine wind tunnel data and if the Reynolds number of the model tests were above a certain minimum Reynolds number $Re = 1 \cdot 10^6$ referred to the average wing chord [6]. The development of modern transonic transport aircraft with new profile shapes, however, has shown that the forced transition of the laminar boundary layer in the wind tunnel model is not sufficient alone any more for determining the behaviour of full scale models [7]. The transport aircraft C-141 is a classical example of this, and relatively drastic distances between the

* By transition, we mean primarily forced transition.

extrapolated wind tunnel data and flight tests, especially regarding the pitch moments, were found [8]. The differences in the pitch moments resulted from the fact that the shock positions and the top side of the wing of the wind tunnel model were different than that of the full scale model. Later on it was found that the differences in the shock position were the result of a flow development over the wing, which is determined by the interaction between a trailing edge separation and the local interference of the compression shock with the turbulent boundary layer. The decisive factor here is that the development of the trailing edge separation, the occurence of separation itself and the propagation of the separated region depend greatly on the boundary layer characteristics with increasing Mach number or increasing angle of attack, and in particular, they depend on the boundary layer thickness ahead of the compression shock [9]. Different possible development forms of separated regions/12 over transonic profiles were described by Pearcey et al in [7].

3.2 Program for determining the influence of Reynolds number and transition

The differences in the shock position which depend on Reynolds number and transition and, therefore, the aerodynamic coefficients, were observed primarily for those wing configurations whose profiles are characterized by a large pressure increase near the trailing edge (Rear loading) and a small Mach number gradient ahead of the shock on the suction side of the profile (Roof Top distribution of pressure). The CAST profiles investigated here have this characteristic feature in the important downstream regions; therefore, measurements at different Reynolds numbers with free and forced transition were carried out with profiles CAST 7 and CAST 10-2, and in the latter case, both the position as well as the roughness of the roughness strips was varied [12]. Table 1 gives details of the program.

The transition strips were made of carborundum grains which were applied both to the pressure side and the suction side of the wing. They extended over the entire span and have a width of about 2.5 mm or 1.25% of wing chord.

3.3 Results

In the following part we will give selected examples to show a summary of the influence on Reynolds number and transition on the flow development over the supercritical profiles. We also wish to validate the data for transfer of results to the large full scale model in a critical model. For this purpose we use the results of profiles CAST 7 and CAST 10-2 because they were available. The totality of the results is given in [12]. /13

3.3.1 Influencing of lift and drag in the investigated angle of attack range

Figure 17 shows the lift and the drag as a function of angle of attack for the profile CAST 7 (SP 120) at a Mach number Ma = 0.70. The Reynolds number and the granularity of the transition strip are the parameters. As can be seen, the influence of these parameters on the lift is relatively small in the lower angle of attack range ($\alpha<4.0°$). The changes caused by Reynolds number in general are somewhat greater than those which result from a variation of the grain diameter. In this angle of attack range the changes in the lift or in the pressure distribution are primarily the consequence of the change in the displacement thickness of the profile. In the upper angle of attack range the influence of Reynolds number and transition is substantially greater. For example, it can be clearly seen that for forced transition at 5% of the profile chord the flow is already separated for the most part. For free transition and Re = $2.3 \cdot 10^6$, it seems to still be completely attached. We will discuss this behavior using the example of even larger Mach numbers.

The drag in the region ahead of the drag increase depends only slightly on the Reynolds number. However, it increases drastically with increasing granularity diameter. In the region of the large drag increase C_W increases with Reynolds number, which in part can be attributed to a trailing edge separation which occurs at the higher numbers.

Figure 18 shows the lift and the drag as a function of angle of attack for the same profile (CAST 7) for a Mach number of Ma = 0.765; the design Mach number is Ma = 0.76. A comparison with Figure 17 shows clearly that the influence of Reynolds number and transition here is substantially greater which is primarily due to the stronger shocks which occur here in the larger pressure gradients and the related increased danger of local separation. We will indi- /14
cate here that the influence of the granularity diameter on the lift behavior is relatively slight. This is due to the fact that the boundary layer, after it has reached a certain thickness, does not cause any substantial changes in the flow development if it is enlarged more.

3.3.2 Flow development as a function of Reynolds number and transition

In the following we will briefly describe the flow development which leads to the strong influencing of the lift and the drag using the results of the profile CAST 10-2 (SP 220). Figure 19 shows the lift and the drag as a function of angle of attack at Mach number Ma = 0.765 once again and free and forced transition. In the case of forced transition the position of the transition strip but not the granularity was varied.

It is remarkable that even in the linear C_A range (Section I) there is a strong dependence of lift on Reynolds number and transition. C_A decreases with increasing Reynolds number whereas by increasing the backward position of the transition strip results in an increase in lift. The resistance increases with decreasing backward position of the roughness strip and increasing Reynolds number, which in part can be attributed directly to the increase in the path lengths of the turbulent boundary layer.

Figure 20 shows the pressure distributions corresponding to several sections I of Figure 19. It can be seen that the compression shock migrates towards the wing trailing edge with increasing backward position of the roughness strip, and towards the shock position

for free transition and Re = $2.35 \cdot 10^6$. The pressure recovery up to the trailing edge increases. For forced transition there is a great thickening and finally a separation of the boundary layer, and the extent of this increases as the transition strip is moved forward. For free transition the flow is attached up to the trailing edge.

The pressure distributions in Figure 20 are good examples for /15
the influence of the initial boundary layer thickness, that is, the boundary thickness ahead of the shock, and the flow development at the wing trailing edge. A displacement of the transition strip to the leading edge of the wing results in a thicker boundary layer ahead of the compression shock in spite of the greater path length of the turbulent boundary layer. This leads finally to the interference of the compression shock with the boundary layer [7], to trailing edge separation and a corresponding displacement of the compression shock in the forward direction. The relatively low Mach number ahead of the shock ($Ma_L \approx 1.20$) indicates that there still is no clear shock-induced separation here [10]. The exact dimensions of the separated region cannot be determined from the pressure distribution in the form available here. A method with which it is possible to determine the development of the separated region of a profile using the pressure distribution was given in [9].

The lift variation in the region of Section II in Figure 19 gives information about the dependence of the size of the separated regions (here with increasing angle of attack) as a function of the initial boundary layer thickness. As can be seen here the lift increase in the case of free transition decreases only gradually to zero for the Reynolds numbers Re = $1.35 \cdot 10^6$ and $2.35 \cdot 10^6$ and when there is a transition strip at 45% of the wing chord. For free transition Re = $3.59 \cdot 10^6$ and in the case of the other positions of the transition strip, this happens abruptly. From this we can conclude that the separated regions, when there is a thick boundary layer ahead of the shock, will propagate much faster with increasing angle of attack than if there is a thin boundary layer.

A similar variation with increase in Mach number was already discussed in [9]. Figure 21a shows the pressure distributions corresponding to Section II of Figure 19 on the suction side of the profile. The pressure variation behind the shock clearly shows the large differences in the propagation of the separated regions. It can be seen that the separated region in the case of free transition and Re = $3.59 \cdot 10^6$ extends from the compression shock up to behind the profile trailing edge. For forced transition, there is a shock-induced separation at 45% of the wing chord with subsequent reattachment and a second separation in the vicinity of the trailing edge. In the case of low Reynolds numbers and free transition, essentially there is a locally limited shock-induced separation. We find here the pressure distribution which is typical for the interference of an initially laminar boundary layer with compression shock: a slight increase in the pressure, caused by the compression waves which emanate from the separating laminar boundary layer, followed by a strong pressure increase at the point where the compression shock intersects the boundary layer which has now become turbulent. Because of its small thickness, it is able to overcome both the pressure increase in the shock as well as the following pressure increase up to the trailing edge, without substantial separation. /16

Cahill in [11] showed that pressure distributions for low Reynolds numbers and initially laminar shock boundary layer interference (transitional interaction) in general agree very well with pressure distributions at substantially higher Reynolds numbers and turbulent interference. Therefore, he suggests an experiment with a small Reynolds number and an initially laminar shock boundary layer interference as one of the possibilities for simulating the flow behavior at high Reynolds numbers. However, as the curve for free transition and Re = $1.35 \cdot 10^6$ in Figure 21a shows, it seems to be important to select the Reynolds numbers in such a way that the dimensions of the initially laminar separation bubble remain as small as possible.

In addition to the pressure distribution on the suction side, Figure 21b shows the C_p distribution on the pressure side of the

profile for several test conditions corresponding to Section II of Figure 19. As can be seen, the flow here encounters an additional /17 acceleration because of the drop in the trailing edge pressure, which then leads to the reduction of the lift shown in Figure 19. We also have superimposed the influence of the position of the transition point of the boundary layer onto the displacement thickness, and, therefore, the related changes in the effective shape. Of course, a similar influencing occurs on the suction side of the profile ahead of the shock, but it is less important for the development of the flow, which leads to the scale effects observed here.

3.3.3 Influencing of characteristic parameters of the profile flow

Figure 22 shows the dimensionless position of the compression shock as a function of the pressure coefficient at the wing trailing edge for different incident flow conditions, for free and forced transitions. It can be seen that independent of the transition type we have essentially a linear relationship between the trailing edge pressure and the shock position. As already shown, the shock migrates upstream with dropping pressure at the trailing edge. It has to select its position in such a manner that behind ıe shock a pressure develops which is compatible with the pressure distribution which has changed because of the boundary layer separation up to the trailing edge. Pearcey already in [10] pointed out this relationship and its analogy with the flow in a supersonic diffuser. The pressure gradient ahead of the compression shock is very small in the critical incident flow regions, as Figures 20 and 21 show. Because the intensity of the compression shock and, therefore, the pressure behind the shock remain almost constant, the matching to the changed trailing edge pressure can only occur in the subsonic region between the shock and the trailing edge. A relatively large change in the shock position is required to achieve this. For a large positive Mach number gradient ahead of the shock, the reduction of the Mach number caused by the shock migration ahead of the shock and the related reduction of the pressure behind the shock contribute to

the matching with the changed trailing edge pressure. The relationship between the shock position and the trailing edge pressure for a profile with a strong positive Mach number gradient is shown in Figure 22 with a dash and dot line (according to [11]). As can be seen, the shock migration is substantially smaller with changing trailing edge pressure than in the case of the CAST profile. The magnitude of the changes in the coefficient of the CAST profiles when the Reynolds number changes and when there is transition is, therefore, essentially a consequence of the "roof top" distribution of the pressure, or of the Mach number on the suction side of the profiles. The occurrence of the scale effects here is essentially a consequence of the sensitivity of the trailing edge separation and its development with respect to changes in the initial boundary layer thickness. /18

Figure 23 shows the trailing edge pressure, shock position and pitch moment directly as functions of the Reynolds number for free and forced transition for the incident flow quantities of Section II in Figure 19. A comparison of the trailing edge pressure for free transition and for forced transition at 15% of wing chord shows a similar dependence on Reynolds number. From this we can conclude that the transition point for free transition and a Reynolds number $Re = 3.1 \cdot 10^6$ has reached a wing chord of about 15%. When the Reynolds number is increased, it migrates further towards the wing leading edge, and, therefore, in the case of forced transition, it migrates ahead of the roughness strip*. If the Reynolds number is increased further, the transition point reaches its most foremost position. After this there is a reduction in the initial boundary layer thickness. According to the discussion above, this must result in an increase in the trailing edge pressure and, therefore, a backwards displacement of the shock.

The shock reacts as described above for all of the test condi- /19

*The result for forced transition at 5% of wing chord indicates that the transition does not here occur here at the position of the roughness strip.

tions investigated here, as the middle diagram of Figure 23 shows. The variation of the pitching moment essentially is a consequence of the change in the shock position. The absolute magnitude, however, depends on the influence of the pressure distribution along the underside of the profile.

3.3.4 Influencing of the buffet and the drag rise boundary

The discussion above, of course, poses the question as to how the flow will develop for much higher flight Reynolds numbers. We will give a brief discussion of the importance of this question.

The buffet boundary is reached (by definition) as soon as the pressure coefficient at the trailing edge goes below the value of $C_p = 0.10$. This value is shown on the left in the left diagram of Figure 23 as a dash and dot line. As can be seen, C_{pHK} lies at 45% of the wing chord above this value in the case of a Reynolds number of $Re = 1.35 \cdot 10^6$ and $Re = 2.35 \cdot 10^6$ and free transition. The pressure coefficient for all of the other test conditions investigated here lies below this value. This means that at Ma = 0.765 and $\alpha_{korr} = 3.51°$ the buffet limit has not yet been reached or has already been exceeded.

Figure 24 shows the drag rise boundary for the profile CAST 7 (SP 120) as a function of the Reynolds number and transition. The cruise flight state for a sweep angle of 18° $C_A = 0.63$ at Ma = 0.76 is indicated by the filled in square. For free transition and $Re = 2.4 \cdot 10^6$ it is below the drag rise boundary. The curves for the larger Reynolds numbers are slightly above this point but still above the theoretical design point Ma = 0.76, $C_A = 0.5824$ (see Figure 11). Artificial transition leads to separation at the low Reynolds number of $Re = 2.4 \cdot 10^6$ as already theoretical calculations in the design of the profile have indicated. For forced transition /20 and increased Reynolds number, the cruise flight state falls right on the drag line boundary for a sweep angle of 18° as measurements have shown.

It was already mentioned that pressure distributions which were determined for low Reynolds numbers and free transition and, therefore, with initial laminar shock-boundary layer interference, such as already occurred in part at Re = $2.4 \cdot 10^6$ (Figure 21) agree very well with results at substantially higher Reynolds numbers [11]. Figure 25 shows a similar behavior for the example of the dependence of the pitching moment on the Reynolds number and transition. As Figure 23 showed, it is representative for the shock position and the trailing edge pressure. We show the wind tunnel results and the flight results of the Lockheed Transport Aircraft C-141 and the wind tunnel data of the profile CAST-7 for free and forced transition. As can be seen, in the case of the C-141, the wind tunnel results for small Reynolds number and free transition agree exceptionally well with the flight data at Reynolds numbers between Re = $35 \cdot 10^6$ and Re = $70 \cdot 10^6$. The wind tunnel data for forced transition and free transition and Reynolds numbers around Re = $8 \cdot 10^6$ on the other hand show a substantial deviation from the flight data. In addition, it is apparent that an extrapolation of these wind tunnel data to higher Reynolds numbers of flight is probably not possible.

The variation of the pitch moment of the profile CAST-7 corresponds essentially to the variation of the pitch moment of the C-141 in the overlapping Reynolds number range. Since the flow development in the wind tunnel models leading to this pitch moment variation is the same in both cases, we can conclude that the flow development over the profile CAST-7, and, therefore, in the other profiles investigated here, will correspond to the development of the flow over the C-141 or the wing of the C-141 even at higher Reynolds numbers. Measurements for the development of the flow over the supercritical /21 profiles were carried out for free transition and a Reynolds number of Re = $2.4 \cdot 10^6$. Very likely we will achieve a good approximation of the results obtained in this way with the results to be expected at higher flight Reynolds numbers, according to the discussion above.

4. SUMMARY

A direct-inverse method for calculating transonic profile flows at a designed cycle based on it for supercritical profiles has been given. Using the method discussed here, three supercritical airfoil profiles were designed for transport aircraft and were tested in the wind tunnel. The measurements not only resulted in very good agreement between the calculation and the experiments, but they also showed that the new profiles satisfy the specified design requirements.

The investigation of the profiles CAST 7 and CAST 10-2 for different Reynolds numbers and free and forced transition shows that the flow development over these profiles in the important incident flow regions depends very greatly on the Reynolds number and the position of the transition strip. This strong dependence results from the large pressure gradient in the vicinity of the profile trailing edge and the related danger of trailing edge separation, as well as the low pressure or Mach number gradient of the compression shock on the suction side of the profile. The strong dependence of the development of the trailing edge separation with increasing Mach number or increasing angle of attack on the initial boundary layer thickness, that is the boundary layer ahead of the compression shock, is the decisive factor here.

The tests of the airfoil profiles were carried out for free transition and a Reynolds number of $Re = 2.4 \cdot 10^6$, with a very small initial boundary layer thickness. We show that it is likely we will /22 obtain a substantial agreement between the results obtained in this way and the expected results for the full scale model at high Reynolds numbers.

5. REFERENCES /23

[1] KUEHL, P.
ZIMMER, H.
The design of airfoil profiles for commercial aircraft with improved high speed flight characteristics. Dornier report No. 74/16 B, 1974

[2] LUDWIEG, H.
LORENZ-MEYER, W.
SCHNEIDER, W.
The transonic wind tunnel of the aerodynamic test facilities Goettingen. Yearbook of the WGLR 1966, P. 145-155

[3] HOTTNER, Th.
LORENZ-MEYER, W.
The transonic wind tunnel of the aerodynamic test facility Goettingen (2nd development stage). Yearbook of the DGLR 1968, P. 235-244

[4] STANEWSKY, E.
Wind tunnel testing of 3 supercritical profiles; test techniques and results for the profile CAST 7 DFVLR/AVA Report 74 C 02, 1974

[5] STANEWSKY, E.
Wind tunnel testing of 3 supercritical profiles: results for the profile CAST 10-2 and CAST 12-1 DFVLR/AVA Report 74 C 14, 1974

[6] HAINES, A. B.
HOLDER, D. W.
PEARCEY, H. H.
Scale effects at high subsonic and transonic speeds and methods for fixing boundary layer transition in model experiments ARC R and M No. 3012, 1957

[7] PEARCEY, H. H.
OSBORNE, J.
HAINES, A. B.
The interaction between local effects at the shock and rear separation AGARD Conference Proceedings No. 35, Paper no. 11, 1968

[8] LOVING, D. L.
Wind Tunnel-flight Correlation of Shock-Induced Separated Flow NASA TN D-3580, 1966

[9] STANEWSKY, E.
LITTLE, B. H.
Studies of separation and reattachment in Transonic Flow AIAA Atmospheric Flight Mechanics Conference, Tullahoma, Tennessee, 1970 AIAA Paper No. 70-541 /24

[10] PEARCEY, H. H.
Shock-induced Separation and its prevention by design and boundary layer control boundary layer and flow control, Vol. 2, Editor G. V. Lachmann, Pergamon Press, New York, 1961, pp 1166-1344

[11] CAHILL, J. F. Simulation of full-scale-flight aerodynamic characteristics by tests in existing transonic wind tunnels AGARD Conference pre-print No. 83 on facilities and techniques for aerodynamic testing at transonic speeds and high Reynolds number, Goettingen, April 1971, paper No. 20

[12] STANEWSKY, E. Sensitivity of a certain group of supercritical profiles with respect to changes in Reynolds number and transition DFVLR/AVA Report 74 A 33, 1974

TABLE 1: Program for investigating the influence of Reynolds number and transition

profile	Ma +	α^{o} +	Re · 10^{6} +	Transition
CAST 7 (SP 120)	0,60 to 0,86	0 to 8	1,36 2,3 3,0	free
	0,70; 0,765 0,80; 0,86		3,6	free
	0,70; 0,765 0,80; 0,86		1,36 2,3 3,0	100 K, 5l #
			1,36 2,3	150 K, 5l
CAST 7	0,70; 0,765 0,80; 0,86	0 to 8	2,3	220 K, 5l 220 K, 15l
CAST 10-2	0,5 to 0,9	-2 to 8	2,3	free
(SP 220)	0,765; 0,80	-2 to 8	2,3 2,3	220 K, 5l 220 K, 15l 220 K, 30l 220 K, 45l
CAST 10-2	0,765; 0,80	-2 to 8	3,0 3,6	220 K, 15l

+ these values of the table are indication values

100 K, 5l means: Transition strips made of No. 100 Karborund at 5% of profile chord

FIGURE 1. Theory of the direct method for calculating the transonic profile flow /26

Transonic potential equation:

$$(K - (\varkappa + 1)\,\Phi_x)\,\Phi_{xx} + \Phi_{\tilde{y}\tilde{y}} = 0 \qquad (1)$$

with $$\tilde{y} = Ma^{2/3}\,\delta^{1/3}\,y$$

and $$K = (1 - Ma^2) / (Ma\,\delta^{2/3})$$

Kinematic flow condition over the profile:

$$\Phi_{\tilde{y}} = f'_{o,u}(x) - \alpha/\delta \qquad (2)$$

Boundary conditions at infinity:

$$\Phi_{\tilde{y}} = \Phi_x = 0 \qquad (3)$$

Kutta condition:

$$\left.\begin{aligned} \Phi|_{\tilde{y}=+0} - \Phi|_{\tilde{y}=-0} &= \gamma_0 \\ \Phi_x|_{\tilde{y}=+0} - \Phi_x|_{\tilde{y}=-0} &= 0 \\ \Phi_{\tilde{y}}|_{\tilde{y}=+0} - \Phi_{\tilde{y}}|_{\tilde{y}=-0} &= 0 \end{aligned}\right\} \qquad (4)$$

Pressure distribution:

$$c_p = -2\,(\delta^{2/3}/Ma^{3/4})\,\Phi_x \qquad (5)$$

Lift coefficient:

$$C_A = (\delta^{2/3}/Ma^{3/4})\,\gamma_0 \qquad (6)$$

FIGURE 2. Theory of the inverse method for calculating the transonic profile flow /27

Irrotational condition:

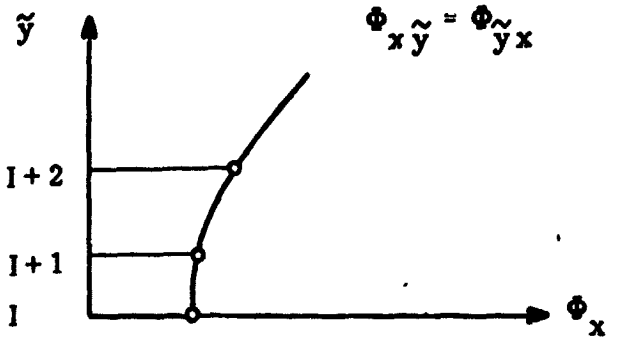

$$\Phi_{x\tilde{y}} = \Phi_{\tilde{y}x} \tag{7}$$

$$\Phi^{n+\frac{1}{2}}_{x\tilde{y}_{i,I}} = -\Phi^{n+\frac{1}{2}}_{x_{i,I}} \frac{2s+t}{s(s+t)} + \Phi^{n}_{x_{i,I+1}} \frac{s+t}{s \cdot t} - \Phi^{n}_{x_{i,I+2}} \frac{s}{t(s+t)} \tag{8}$$

where

$$\Phi^{n+\frac{1}{2}}_{x_{i,I}} = \omega_1 \bar{\Phi}_x + (1 - \omega_1) \Phi^{n}_{x_{i,I}}$$

and $\bar{\Phi}_x$ is the given pressure distribution

Integration:

$$\Phi^{n+\frac{1}{2}}_{\tilde{y}_{i,I}} = \int_{x_0}^{x_i} \Phi^{n+\frac{1}{2}}_{x\tilde{y}_{i,I}} dx + \Phi_{\tilde{y}}\Big|_{x = x_0} \tag{9}$$

$$\Phi^{n+1}_{\tilde{y}_{i,I}} = \omega_2 \Phi^{n+\frac{1}{2}}_{\tilde{y}_{i,I}} + (1 - \omega_2) \Phi^{n}_{\tilde{y}_{i,I}} \tag{10}$$

is substituted in Equation (2).

FIGURE 3

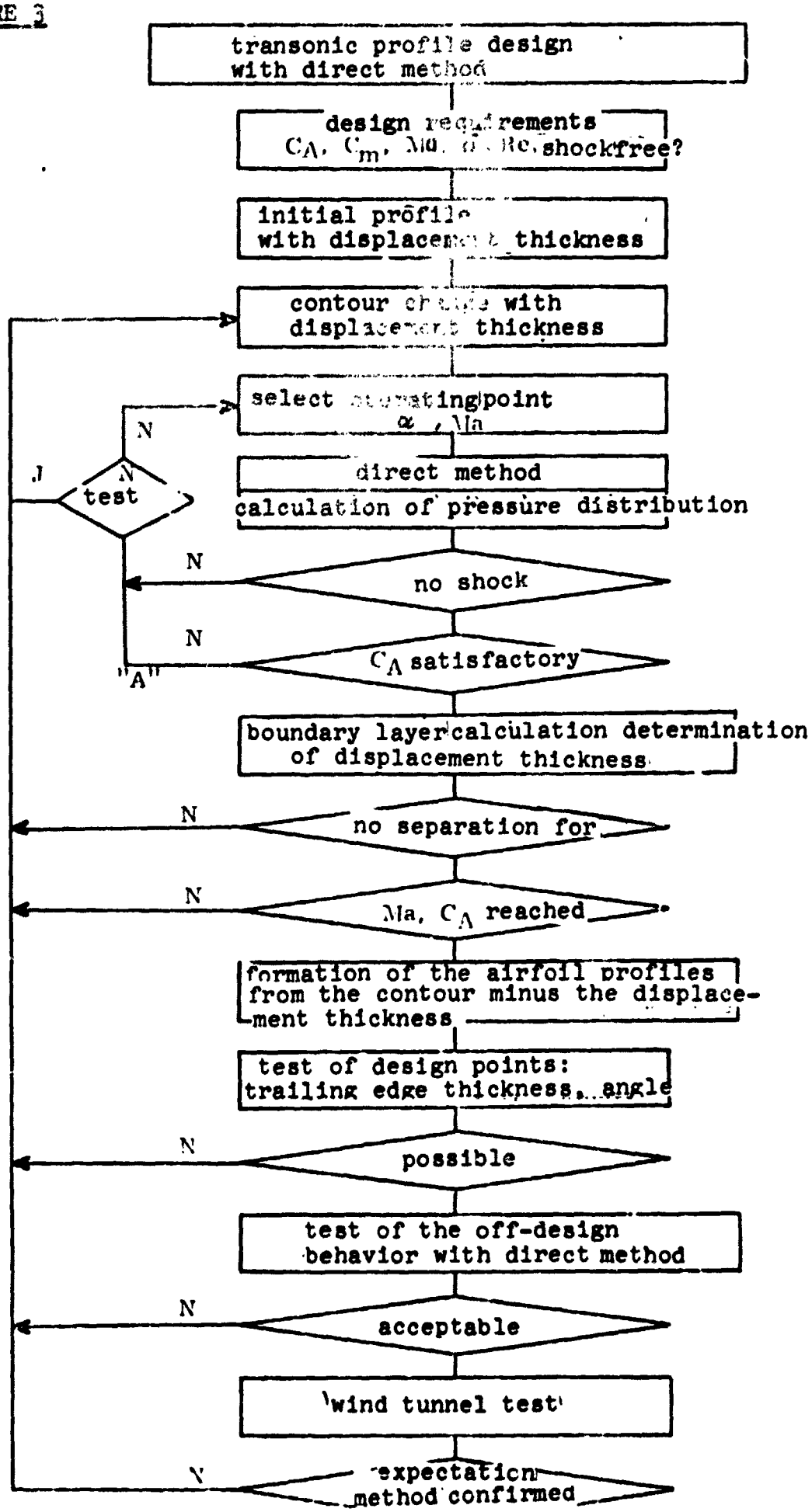
transonic profile design with direct method
design requirements C_A, C_m, Ma, Re, shockfree?
initial profile with displacement thickness
contour change with displacement thickness
select starting point α, Ma
direct method calculation of pressure distribution
test
N
J
N
no shock
N
C_A satisfactory
"A"
boundary layer calculation determination of displacement thickness
N
no separation for
N
Ma, C_A reached
formation of the airfoil profiles from the contour minus the displacement thickness
test of design points: trailing edge thickness, angle
N
possible
test of the off-design behavior with direct method
N
acceptable
wind tunnel test
N
expectation method confirmed

/28

FIGURE 4

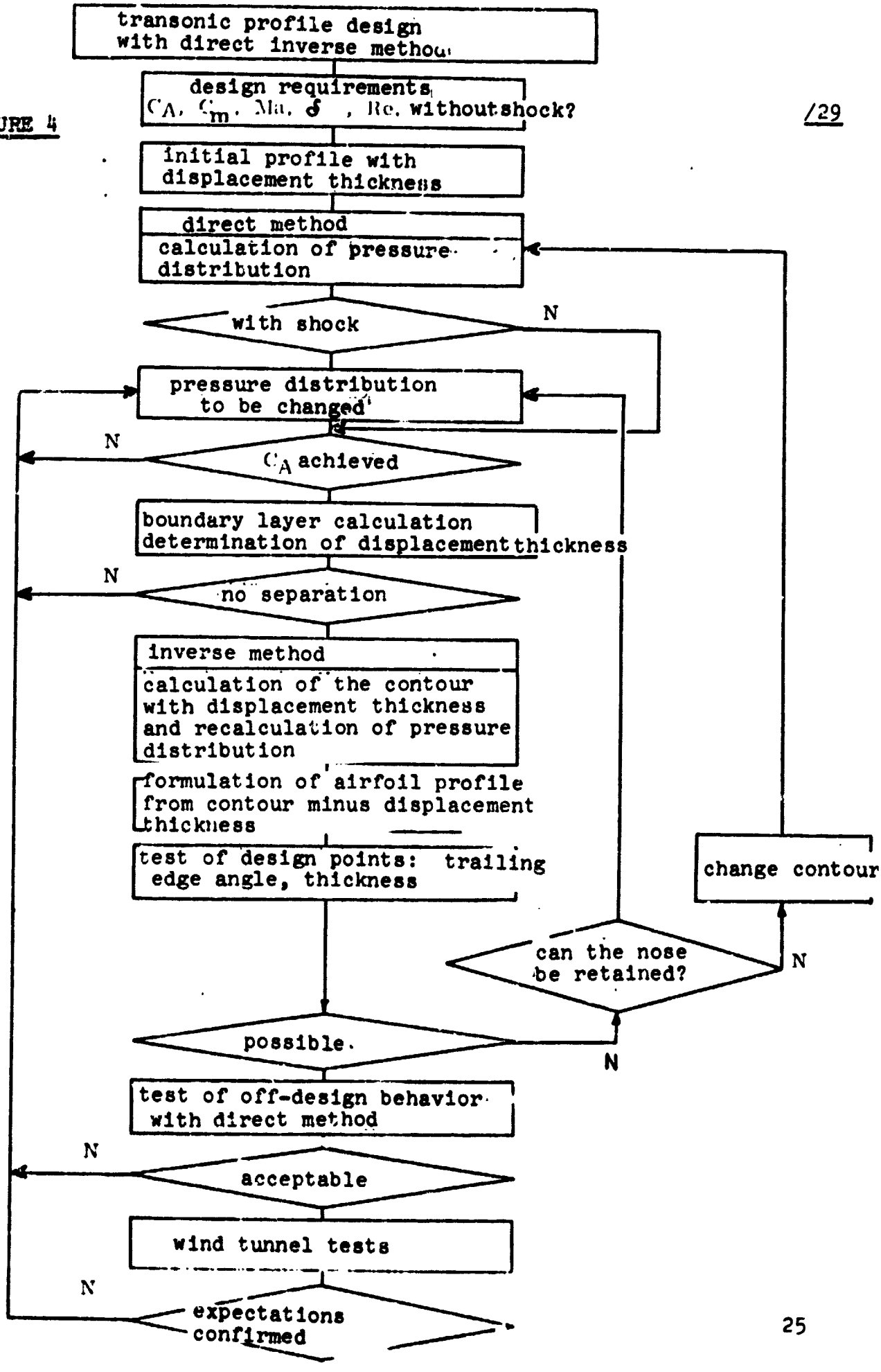
transonic profile design with direct inverse method
design requirements C_A, C_m, Ma, δ, Re, without shock?
initial profile with displacement thickness
direct method
calculation of pressure distribution
with shock
N
pressure distribution to be changed
N
C_A achieved
boundary layer calculation determination of displacement thickness
N
no separation
inverse method
calculation of the contour with displacement thickness and recalculation of pressure distribution
formulation of airfoil profile from contour minus displacement thickness
test of design points: trailing edge angle, thickness
change contour
can the nose be retained?
N
possible.
N
test of off-design behavior with direct method
N
acceptable
wind tunnel tests
N
expectations confirmed

/29

FIGURE 5: AIRBUS BASIC AIRFOIL

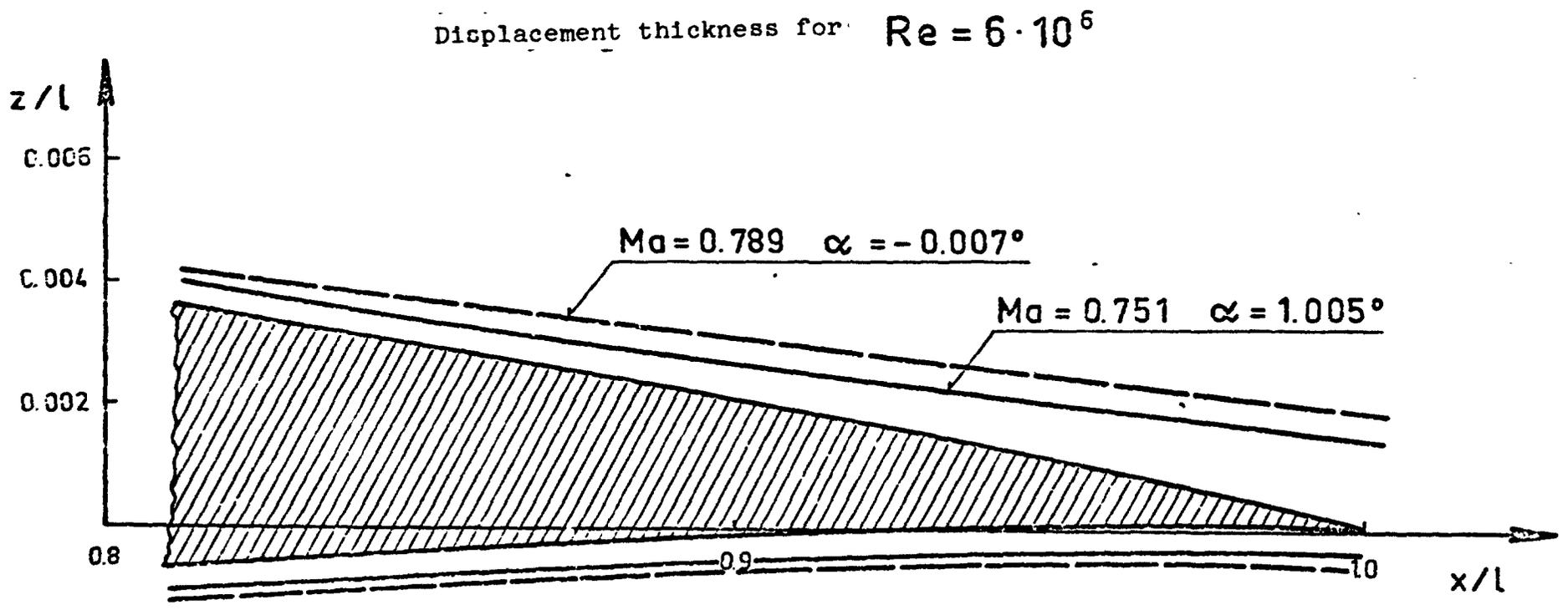

FIGURE 6:

AIRBUS PROFILE

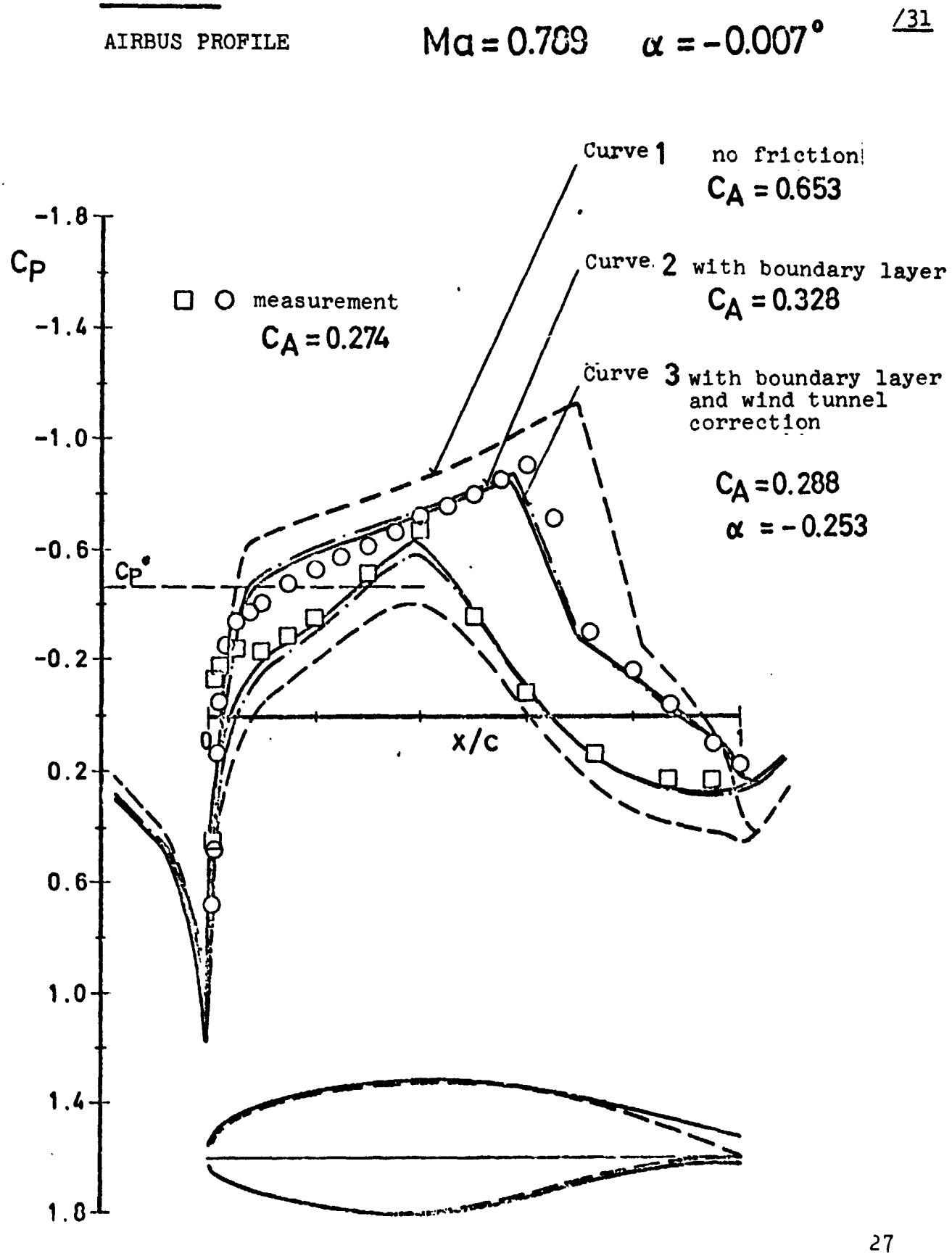

FIGURE 7: DESIGN POINTS AND DRAG RISE BOUNDARY OF THE BASE PROFILE

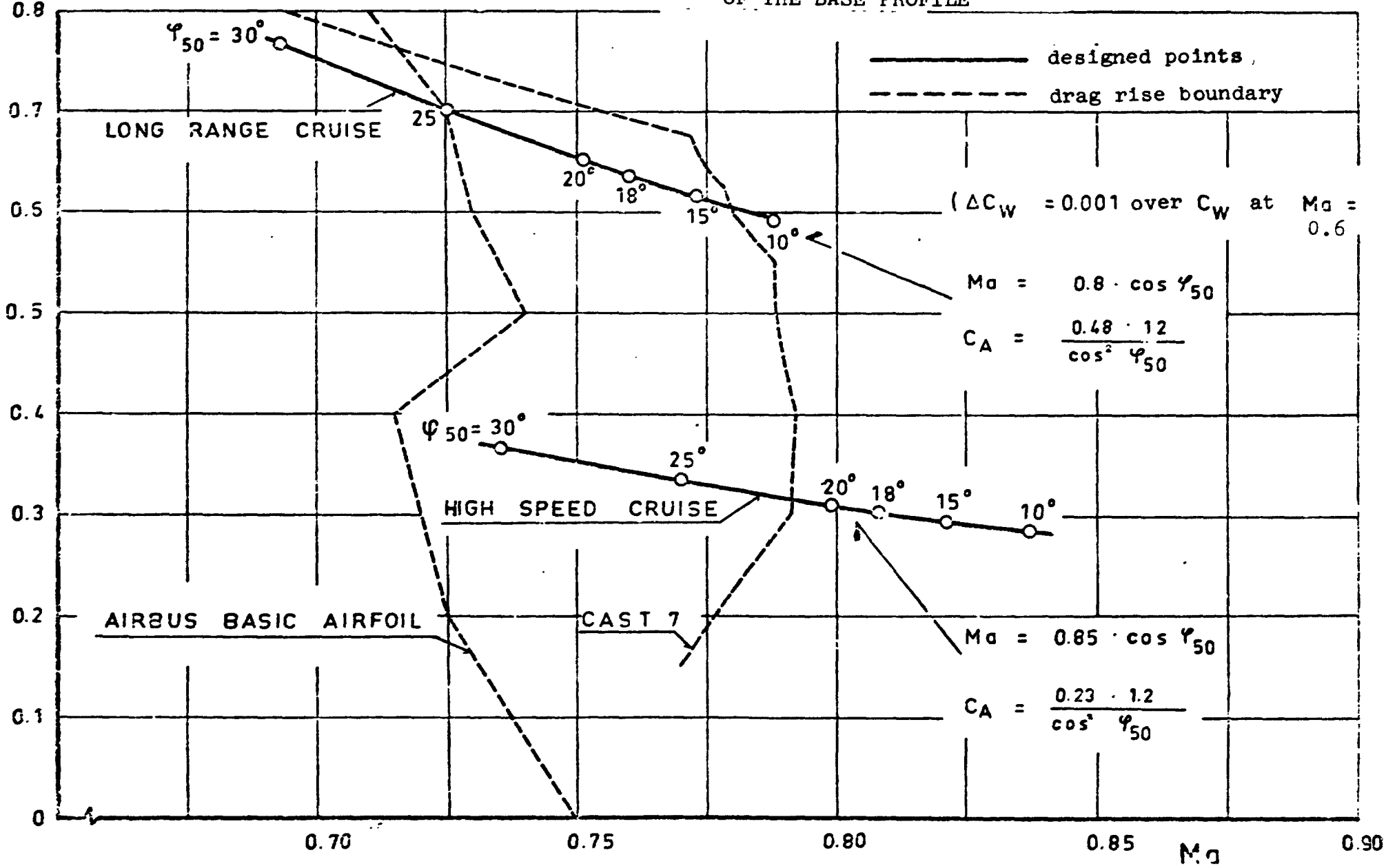

FIGURE 8: TRANSONIC PROFILE DESIGN CHARACTERISTICS

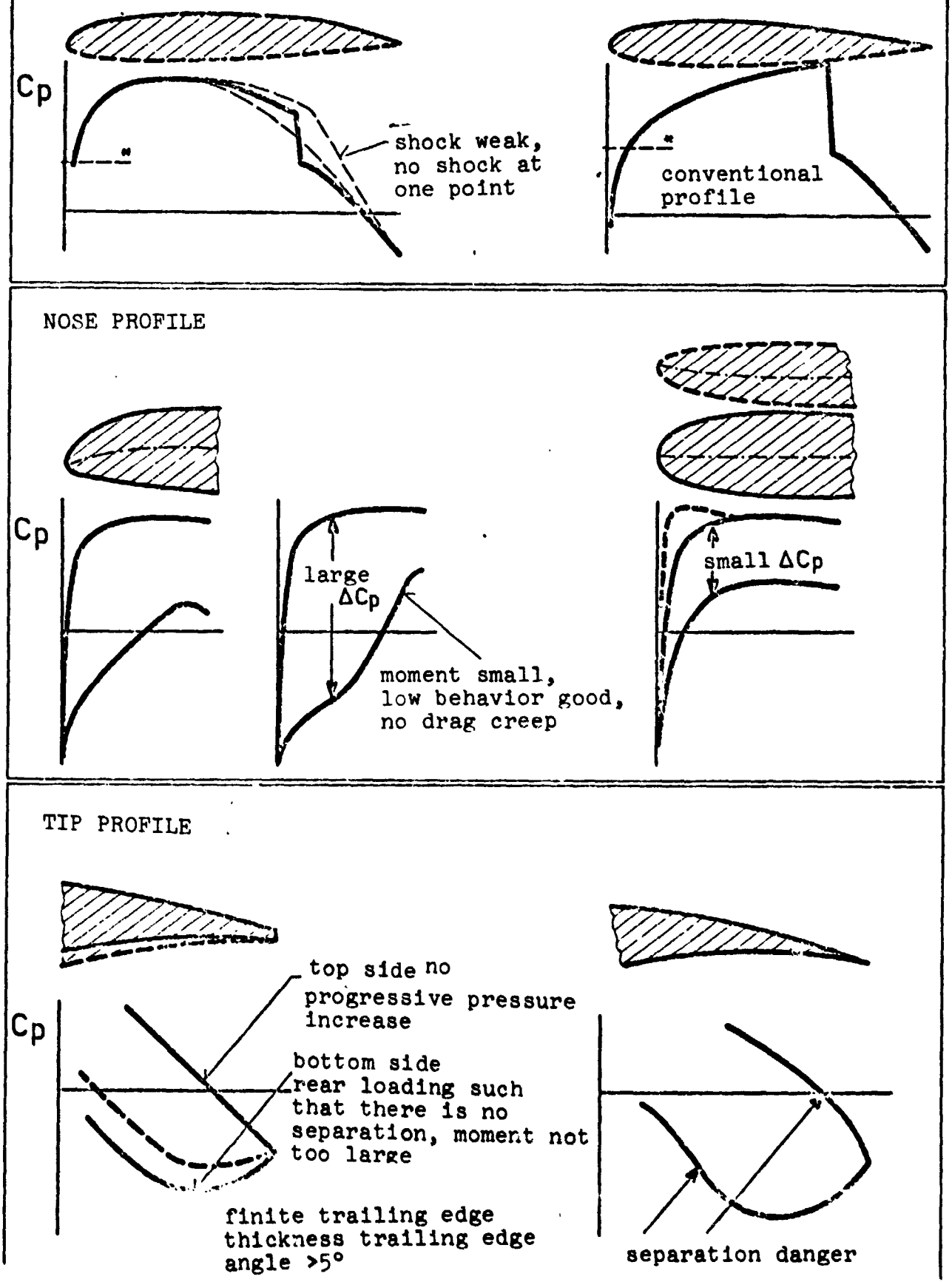

FIGURE 9: DESIGNED AND MEASURED PROFILES /34

PROFILE CAST 7 max. profile thickness 11.8%
thickness backward displacement 35%
trailing edge thickness 0.5%

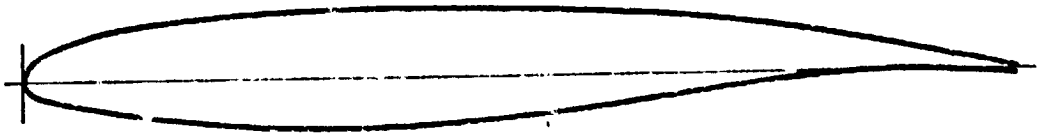

PROFILE CAST 10-2 max. profile thickness 12.1%
thickness backward displacement 45%
trailing edge thickness 0.5%

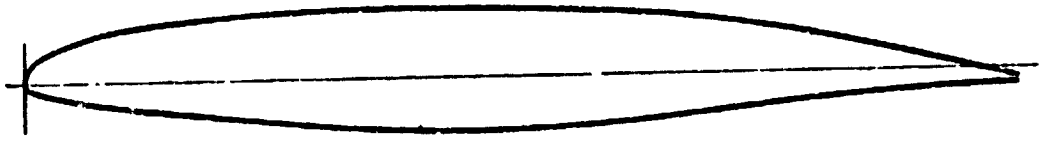

PROFILE CAST 12-1 max. profile thickness 12%
thickness backward displacement 40%
trailing edge thickness 0.5%

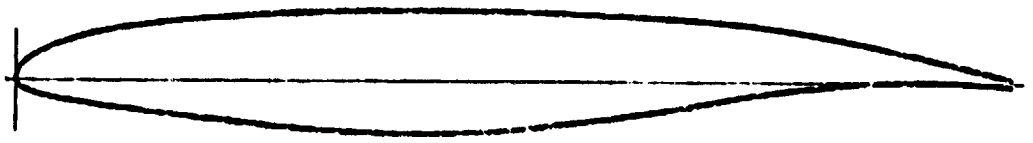

FIGURE 10: CONFIGURATION OF THE MODEL AVA TRANSONIC TUNNEL

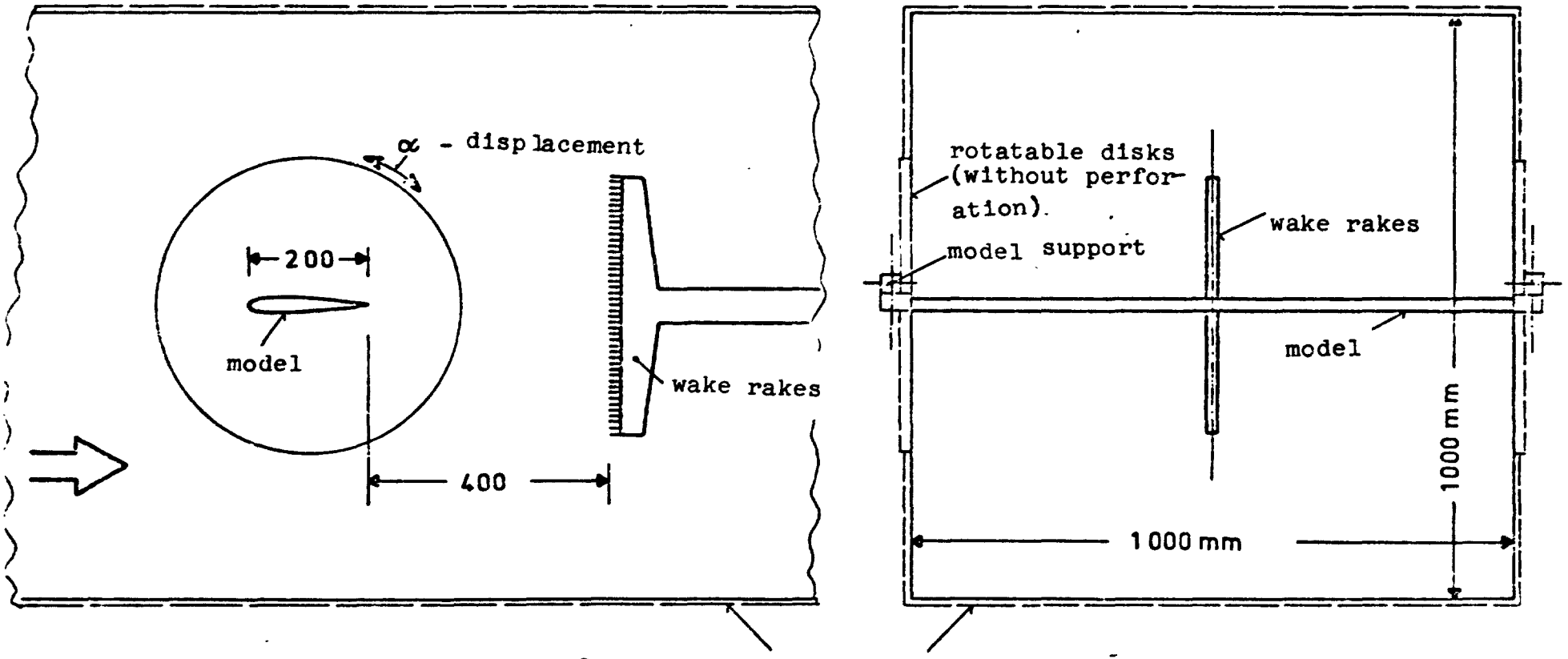

FIGURE 11: PRESSURE DISTRIBUTIONS AT THE DESIGNED POINT /36

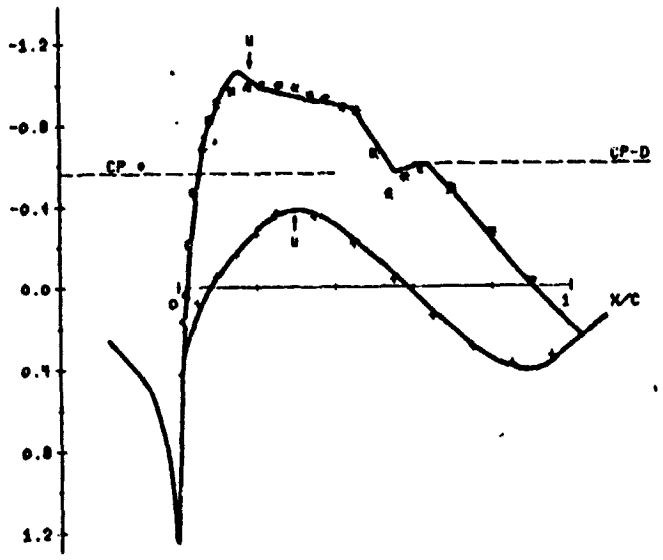

PROFILE CAST 7
boundary layer laminar-turbulent Re = $2.4 \cdot 10^6$
MA = 0.7600
ALFA = 0.3000
C_A = 0.5824

——calculation
+* measurement, α = 2.0°

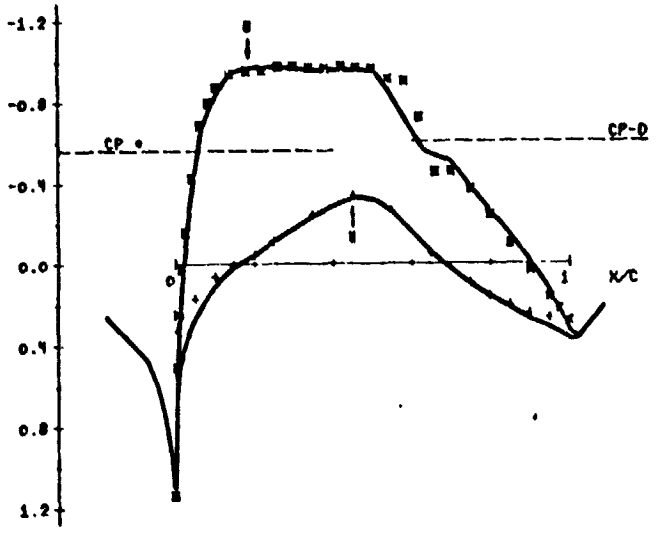

PROFILE CAST 10-2
boundary layer laminar-turbulent Re = $2.4 \cdot 10^6$
MA = 0.7600
ALFA = 0.3000
C_A = 0.5948

——calculation
+* measurement, α=2.01°
MA=0.764

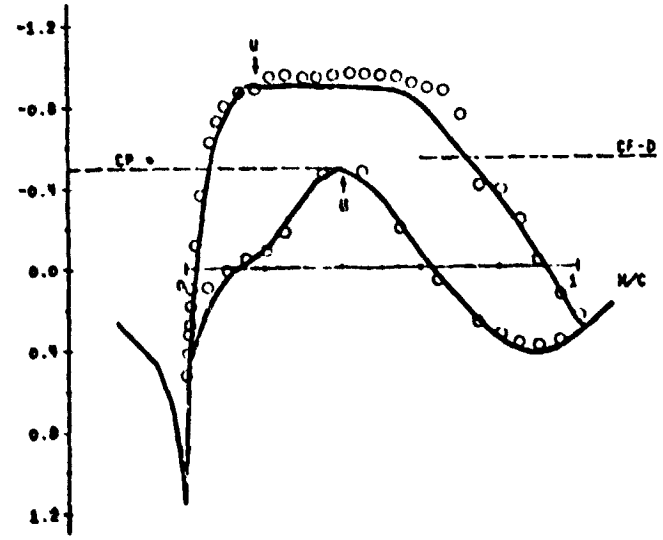

PROFILE CAST 12-1
boundary layer laminar-turbulent Re = $2.4 \cdot 10^6$
MA = 0.7800
ALFA = 0.1900
C_A = 0.5940

——calculation
o measurement, α=2.0°
C_A=0.6274
MA=0.784

FIGURE 12a: CAST 7

Measurement at $Re = 2.4 \cdot 10^6$

/37

$\alpha = 2°$

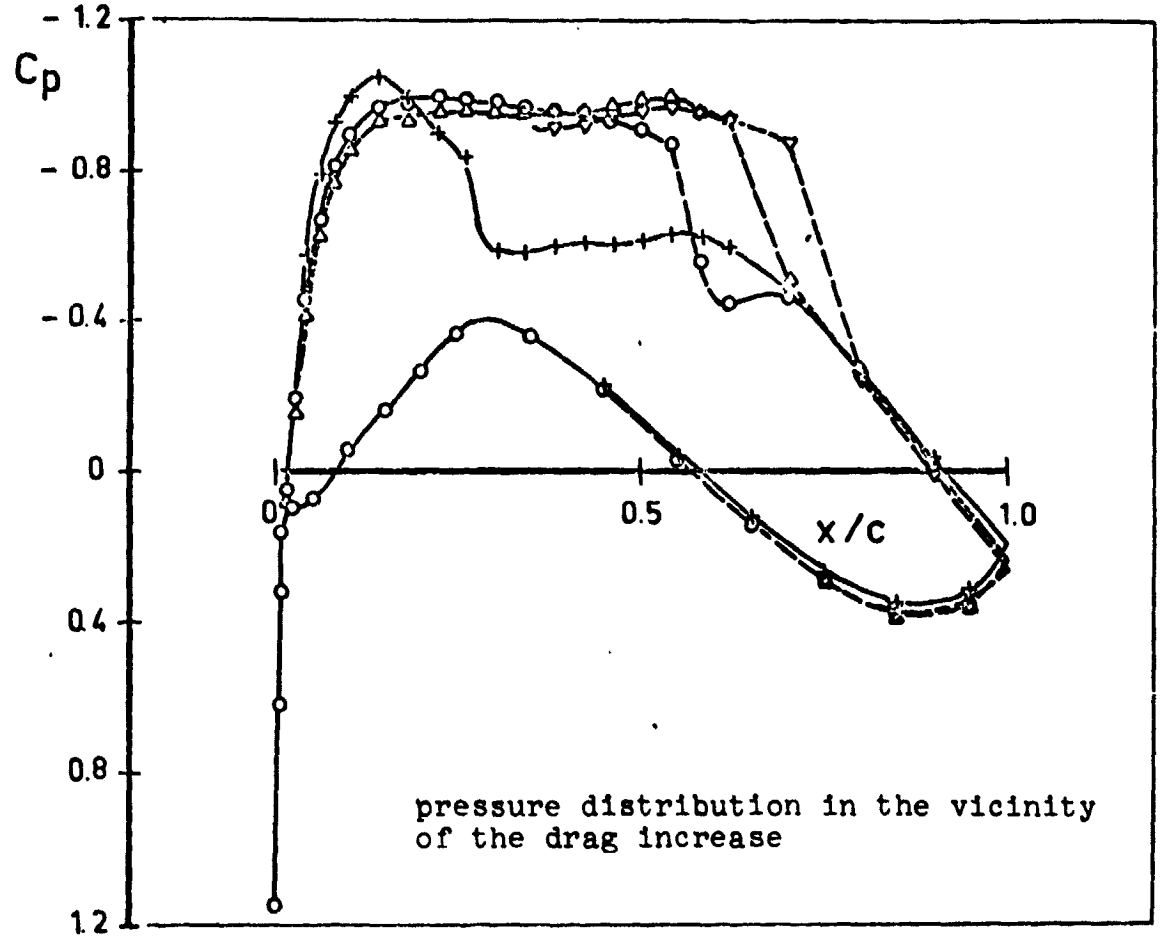

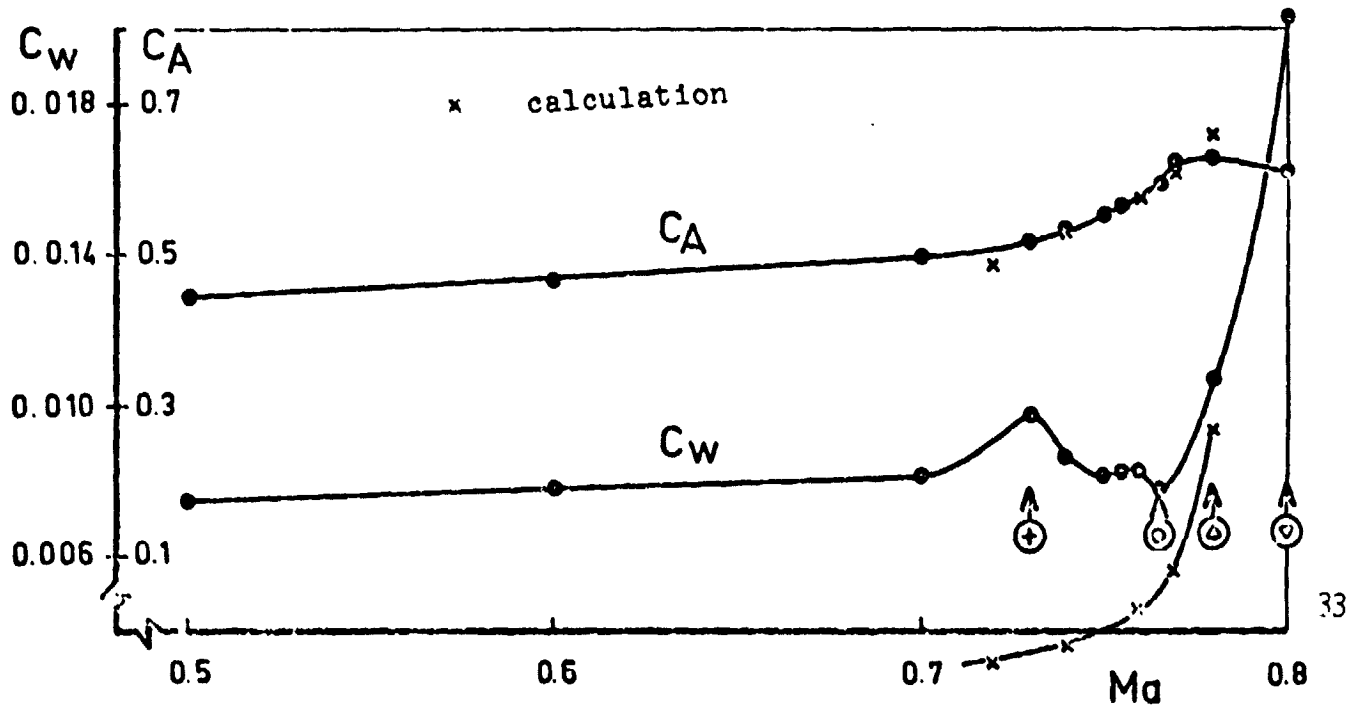

FIGURE 12b: CAST 10 - 2

Measurement at $Re \approx 2.3 \cdot 10^6$

/38

$\alpha = 2°$

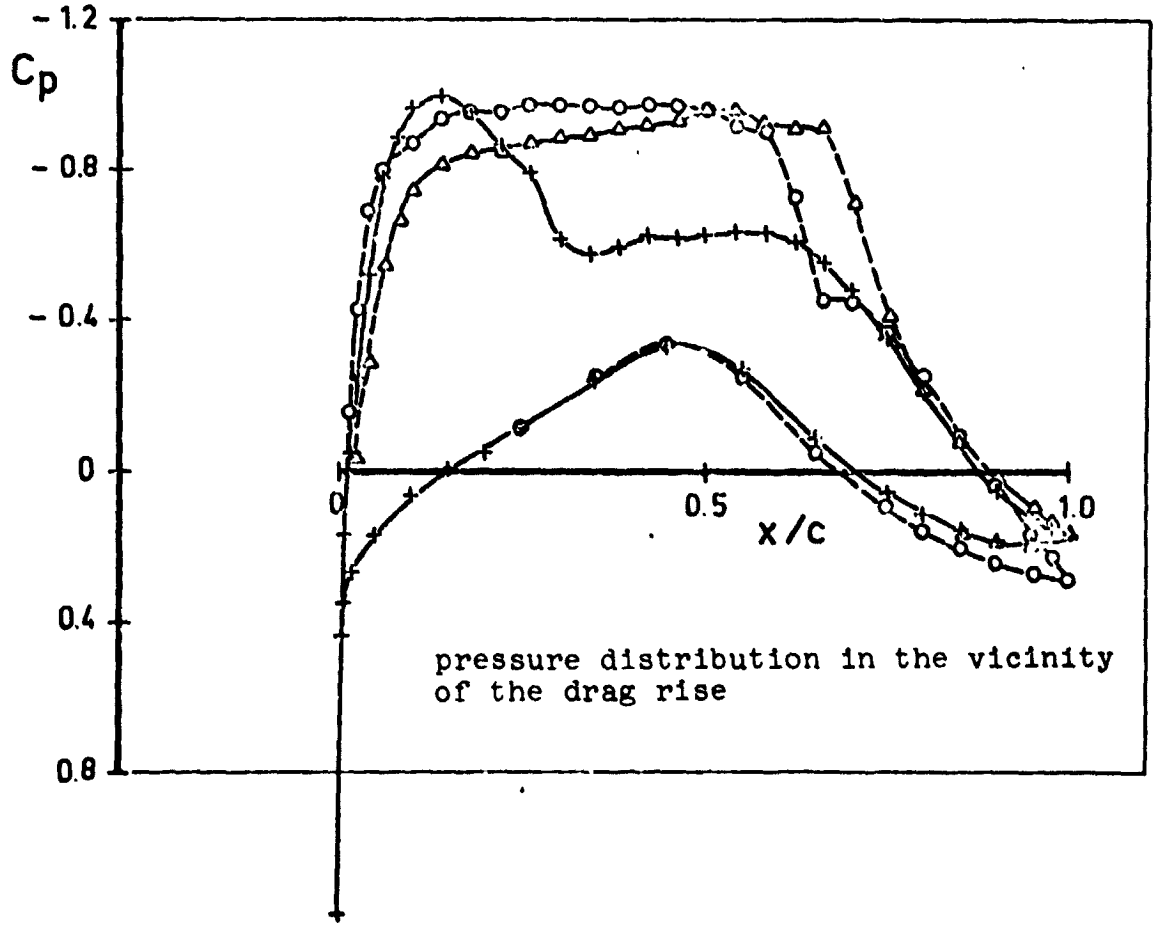

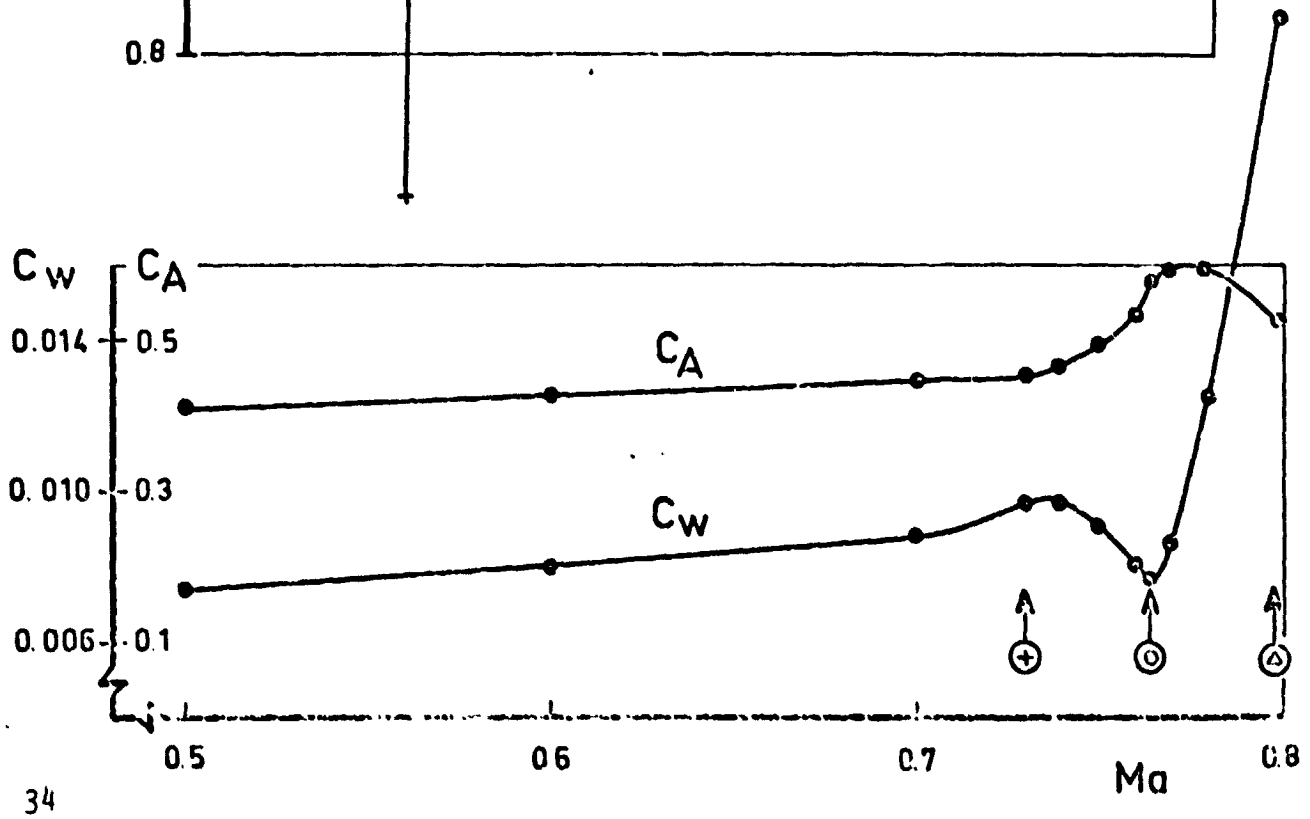

FIGURE 12c: CAST 12 - 1

Measurement at $Re \approx 2.3 \cdot 10^6$

$\alpha = 2°$

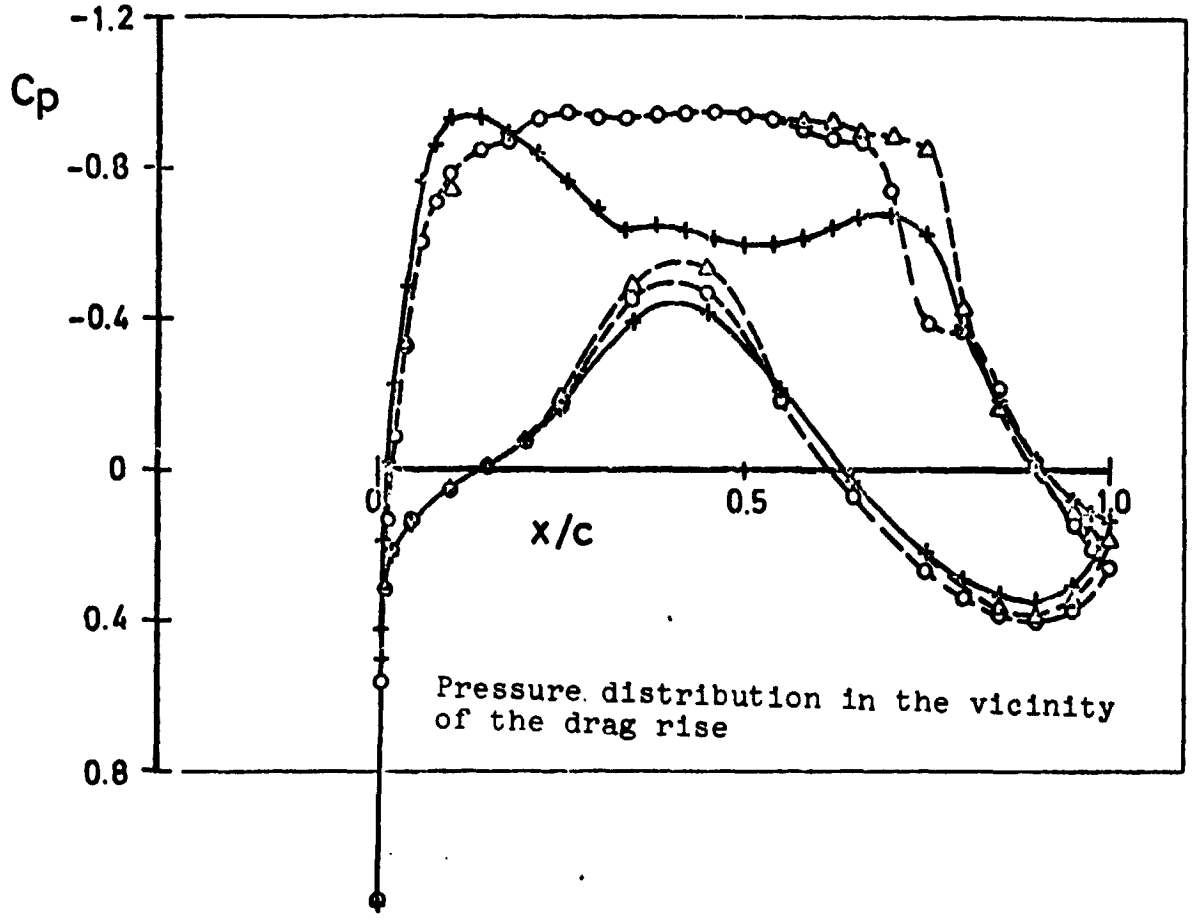

Pressure distribution in the vicinity of the drag rise

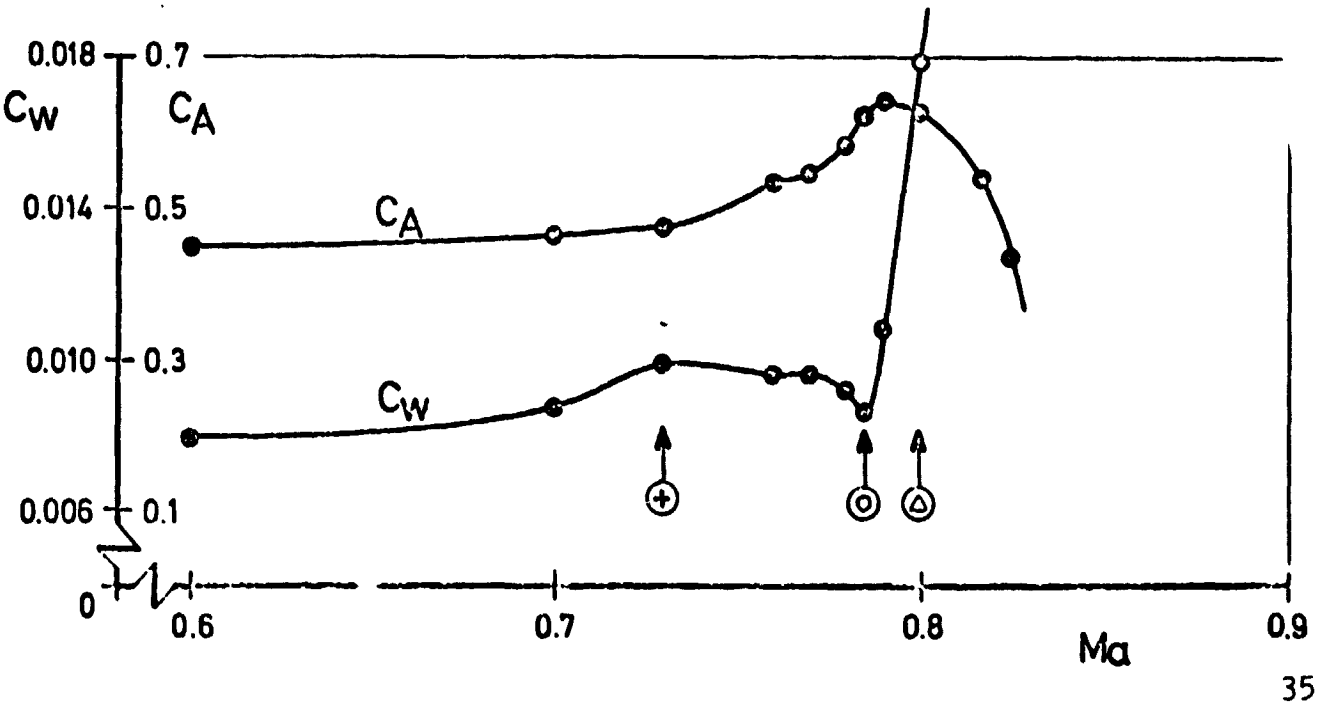

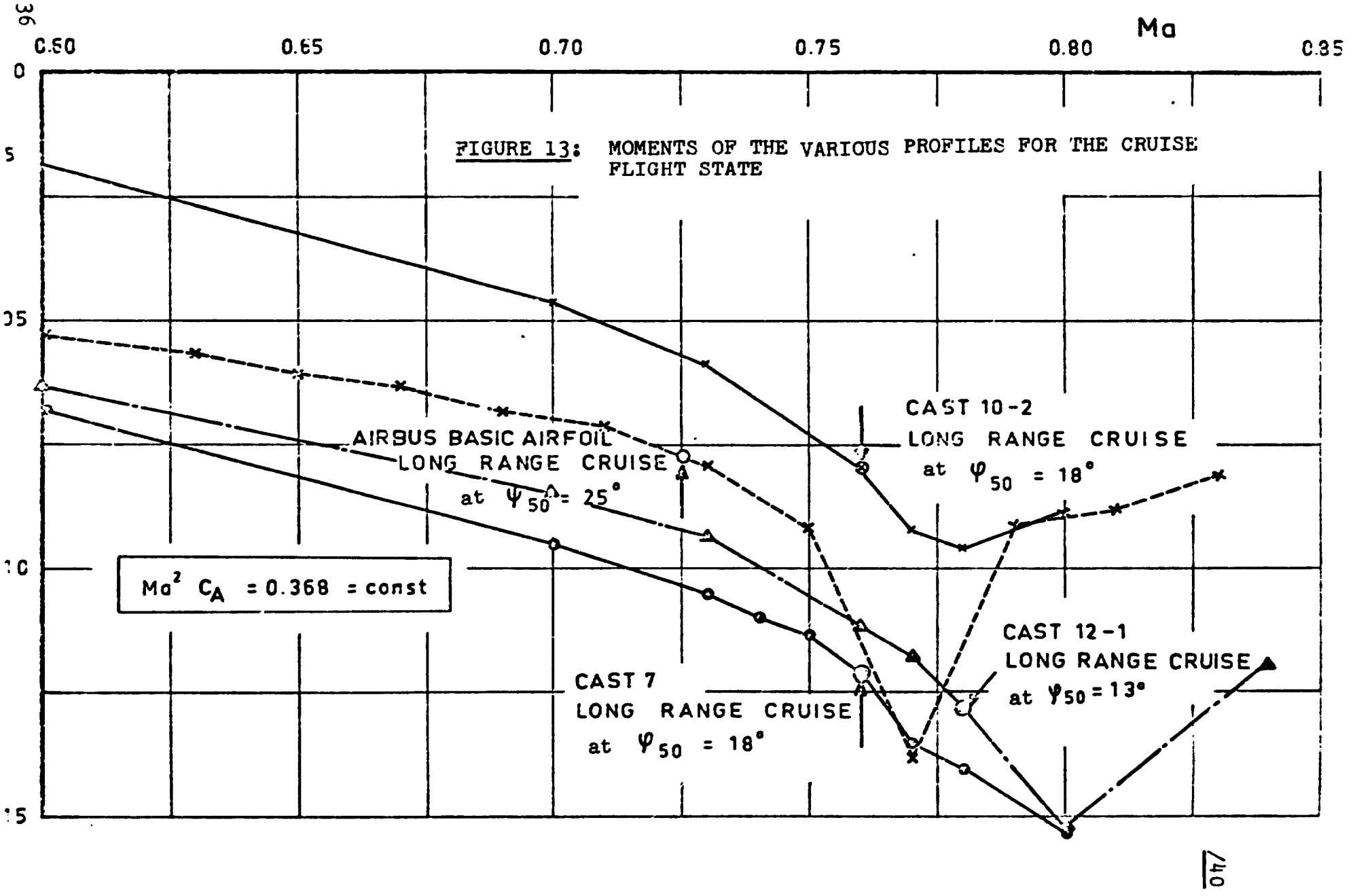

FIGURE 13: MOMENTS OF THE VARIOUS PROFILES FOR THE CRUISE FLIGHT STATE

FIGURE 14: NEUTRAL POINT POSITION OF THE VARIOUS PROFILES IN THE CRUISE FLIGHT STATE

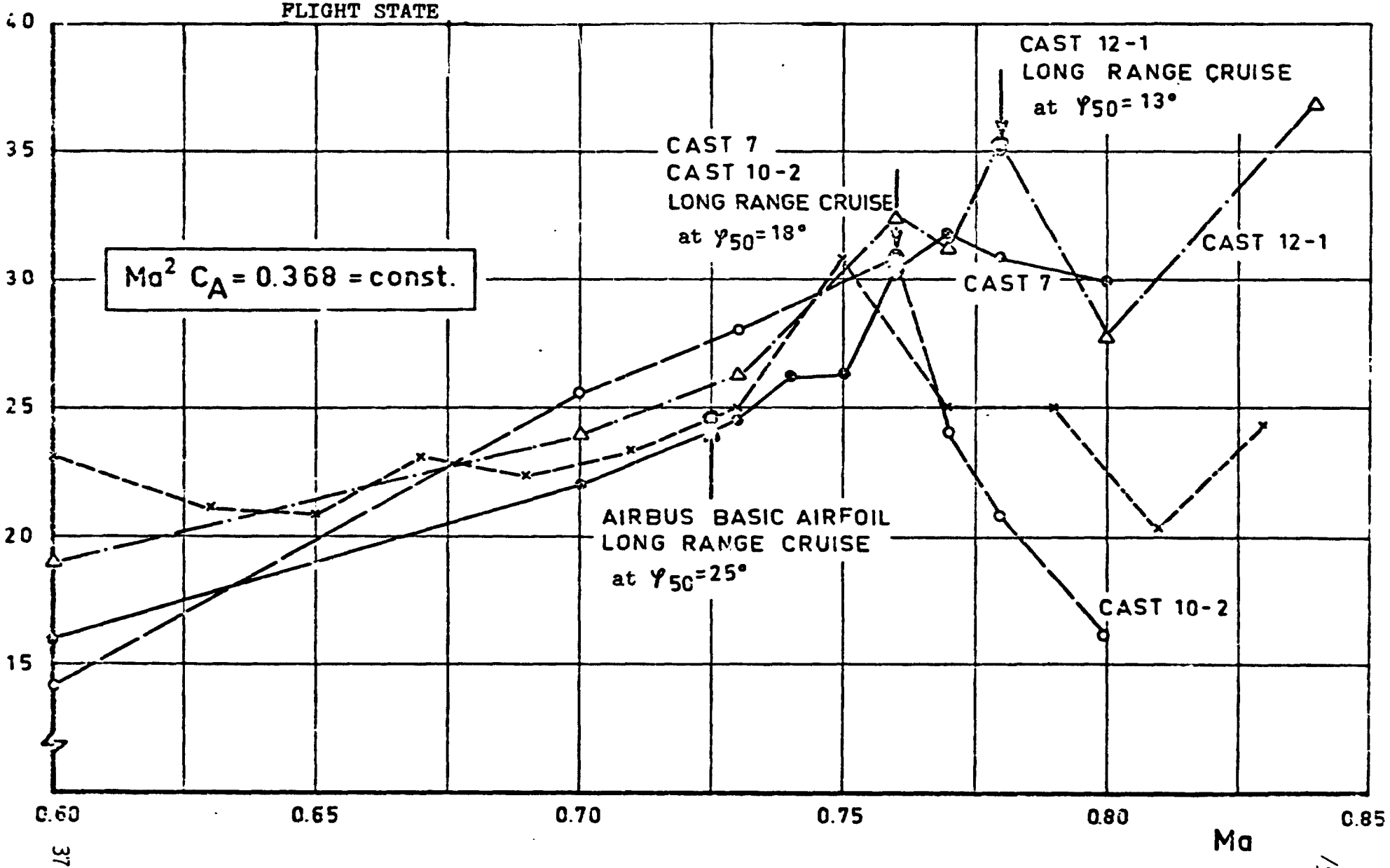

11/11

FIGURE 15: DRAG RISE BOUNDARY AS A FUNCTION OF C_W at Ma = 0.6

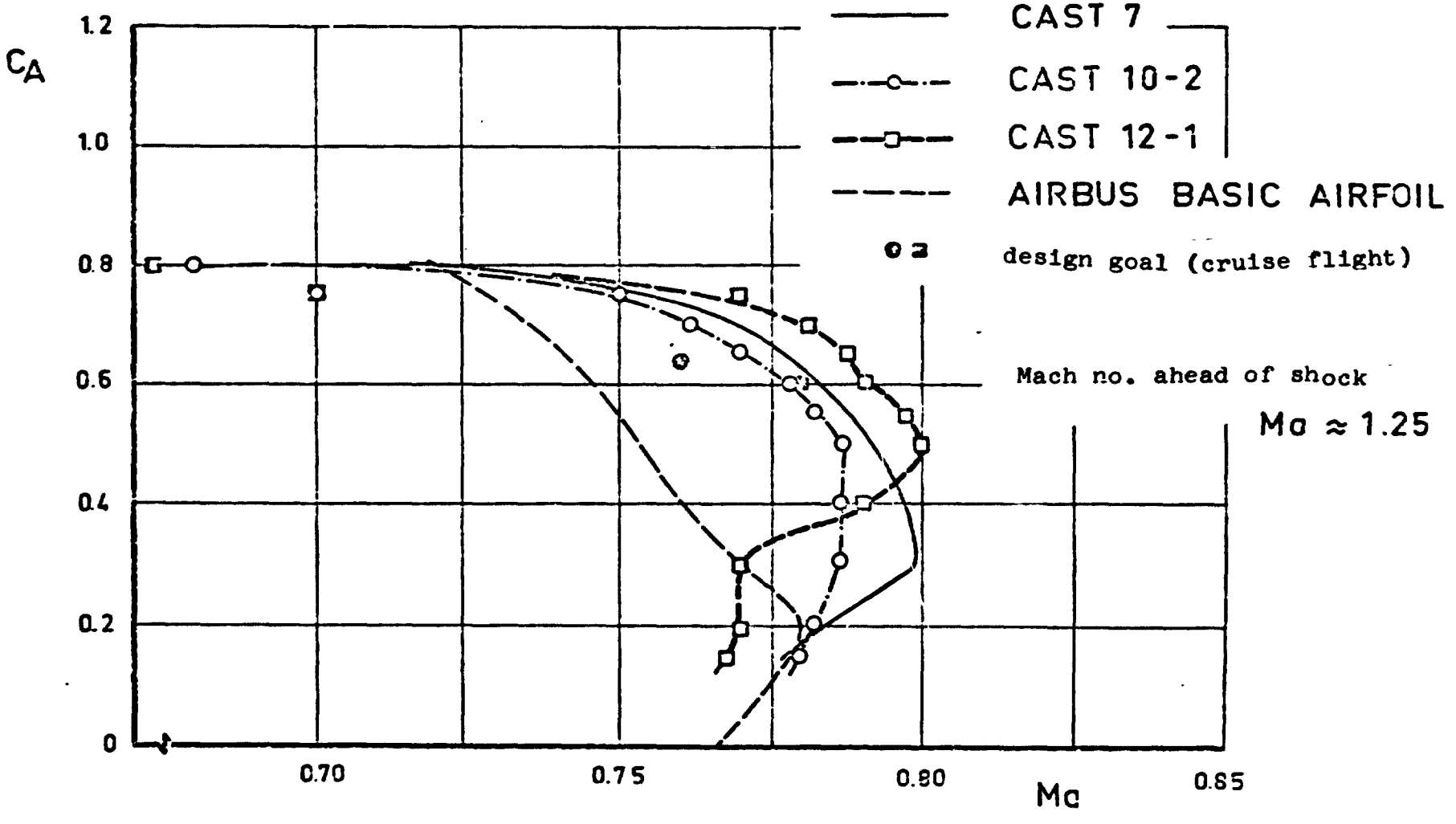

/42

FIGURE 16: BUFFET BOUNDARIES:

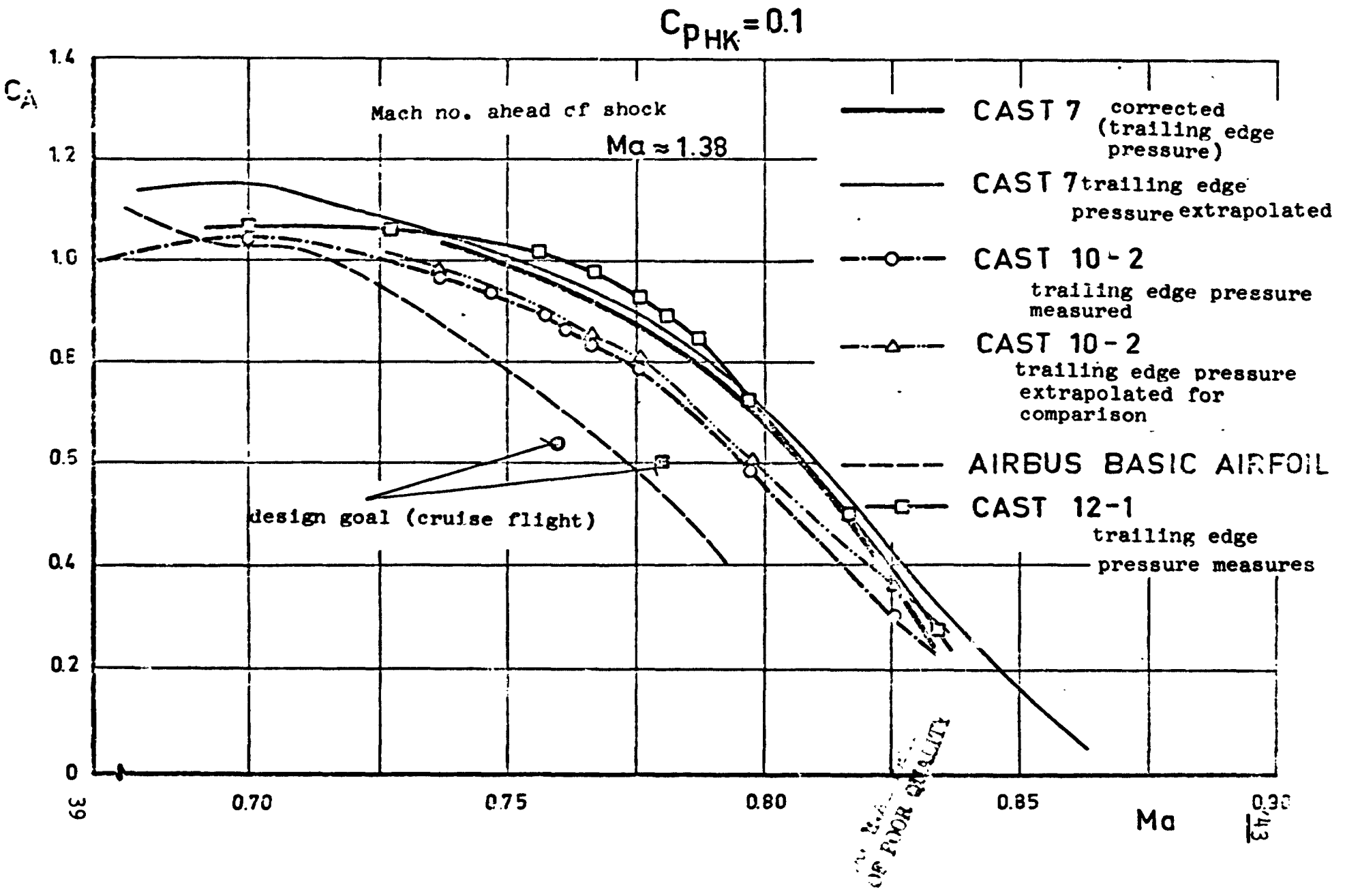

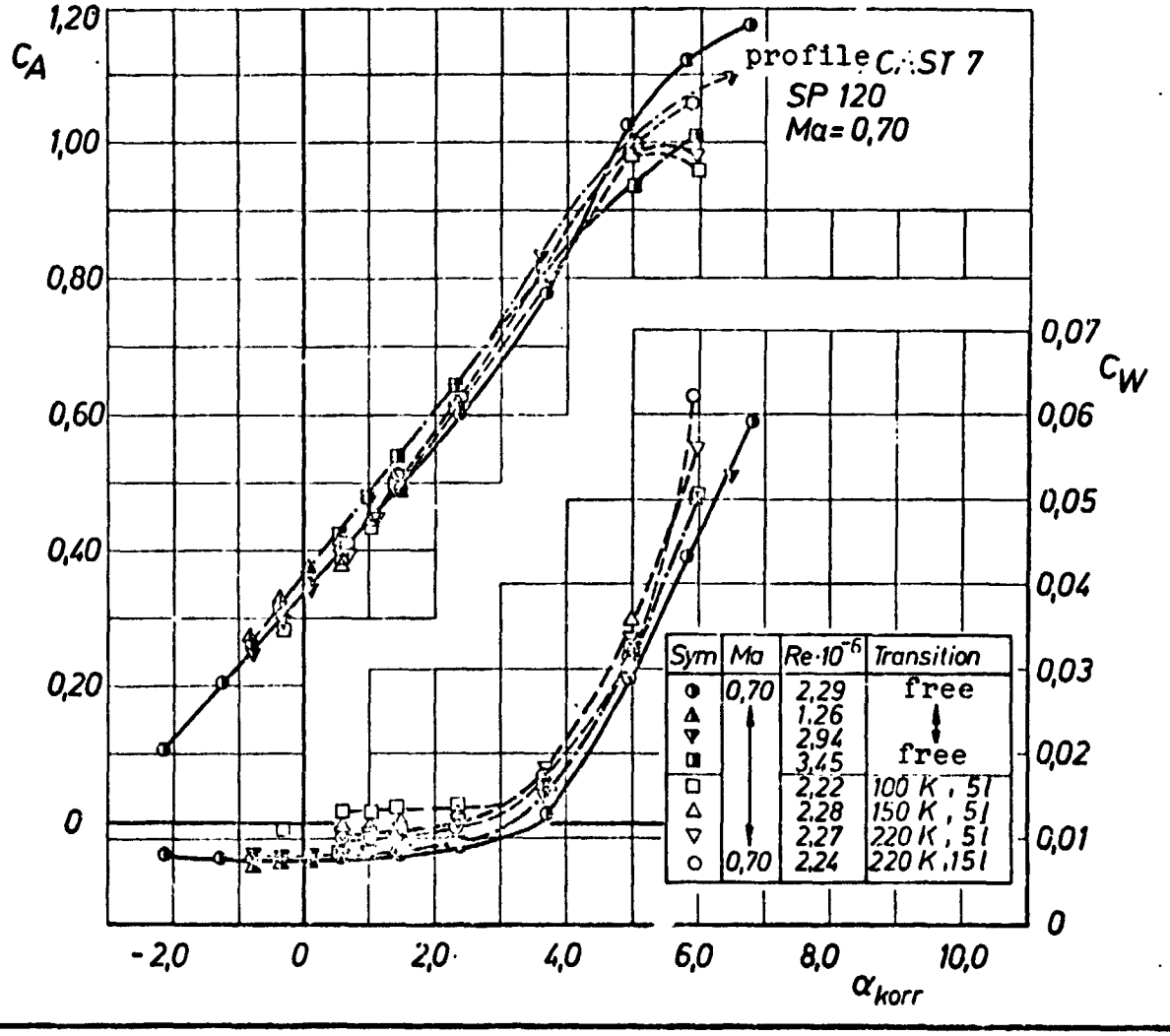

FIGURE 17: Influence of Reynolds number and transition on the lift and the drag Ma = 0,70 profile CAST 7 , SP 120)

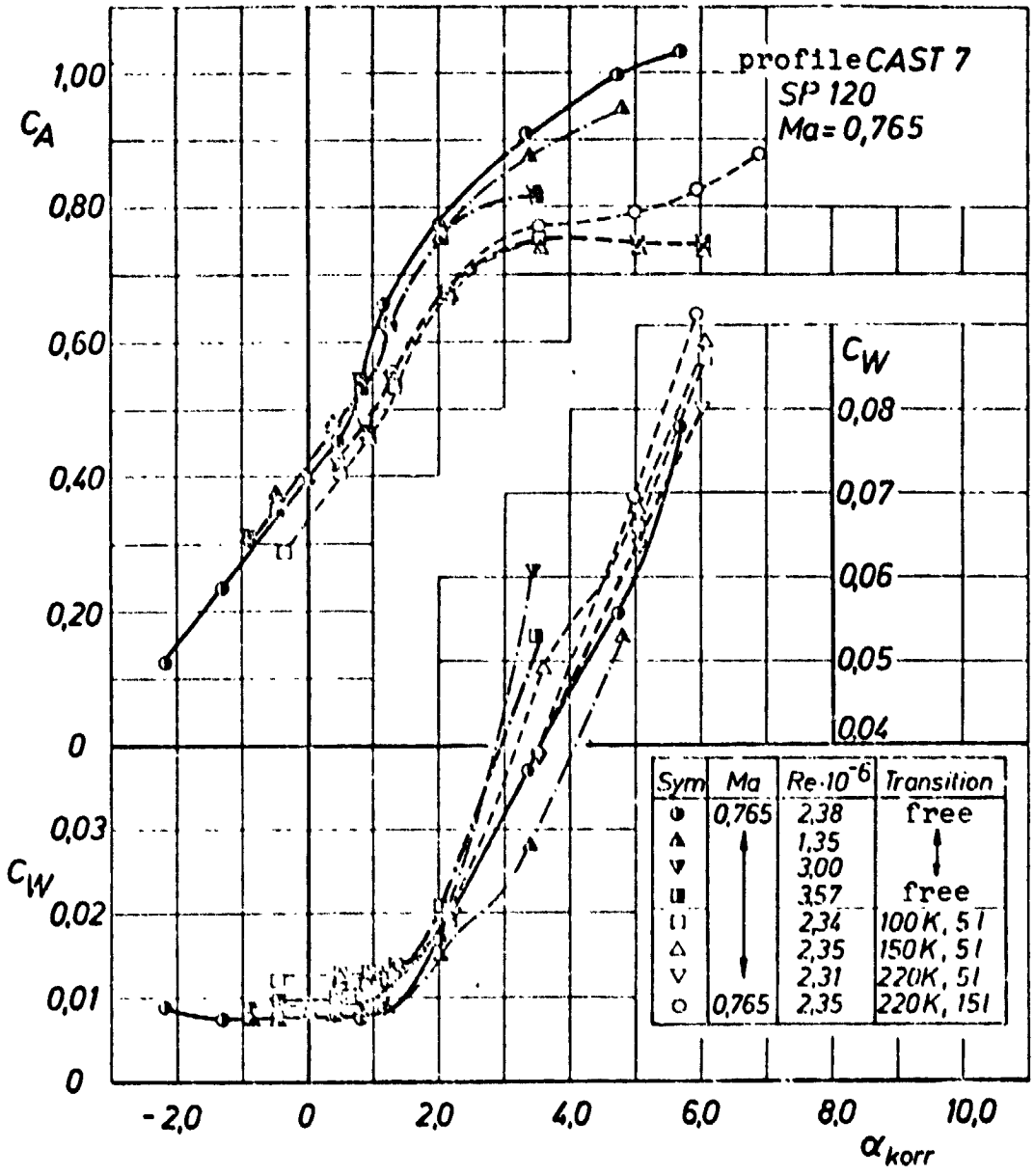

FIGURE 18: Influence of Reynolds number and transition on lift and drag Ma = 0,765 profile CAST 7, SP 120 l

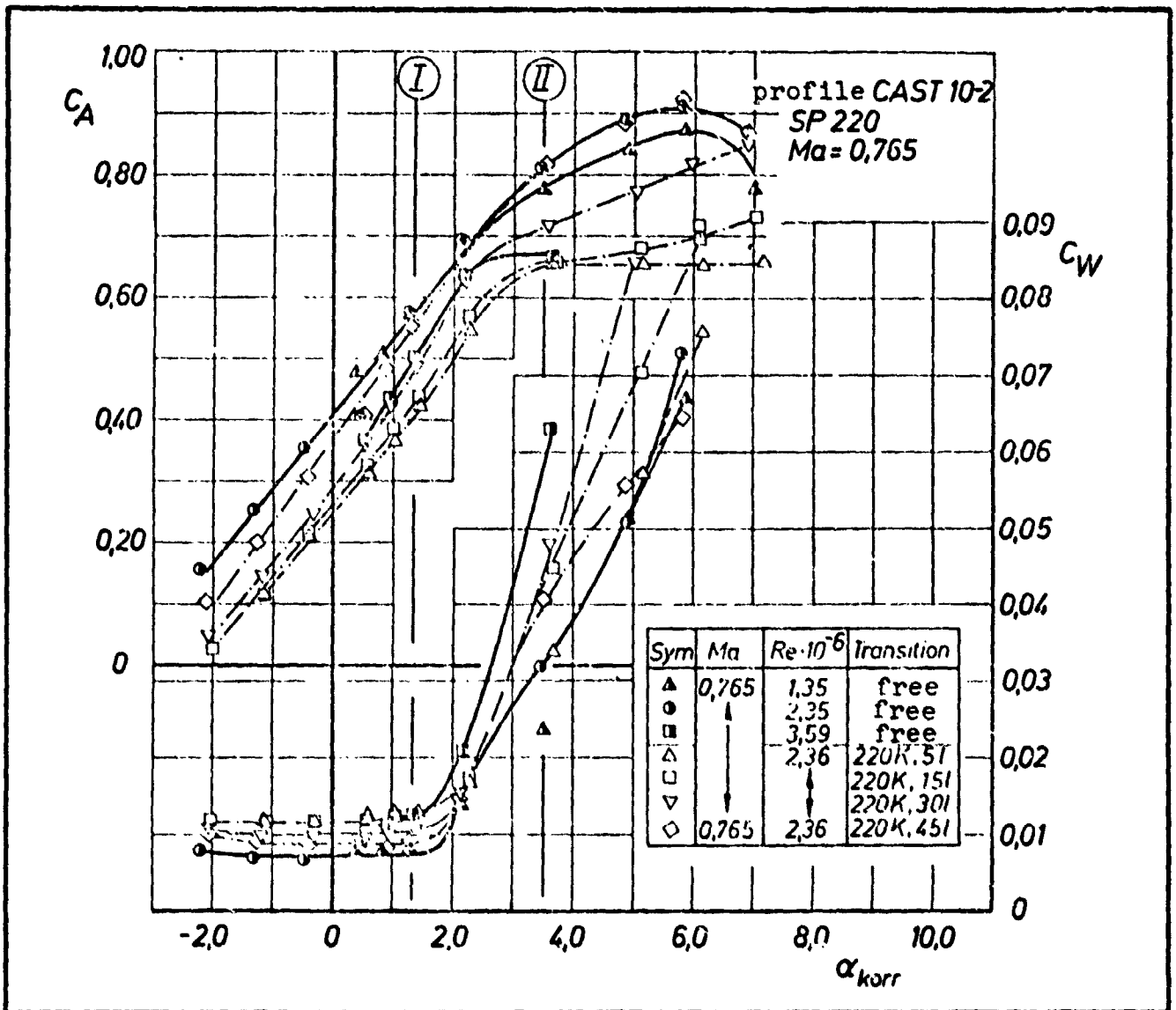

FIGURE 19: Influence of Reynolds number and transition on lift and drag Ma = 0,765 profile CAST 10-2, SP 220)

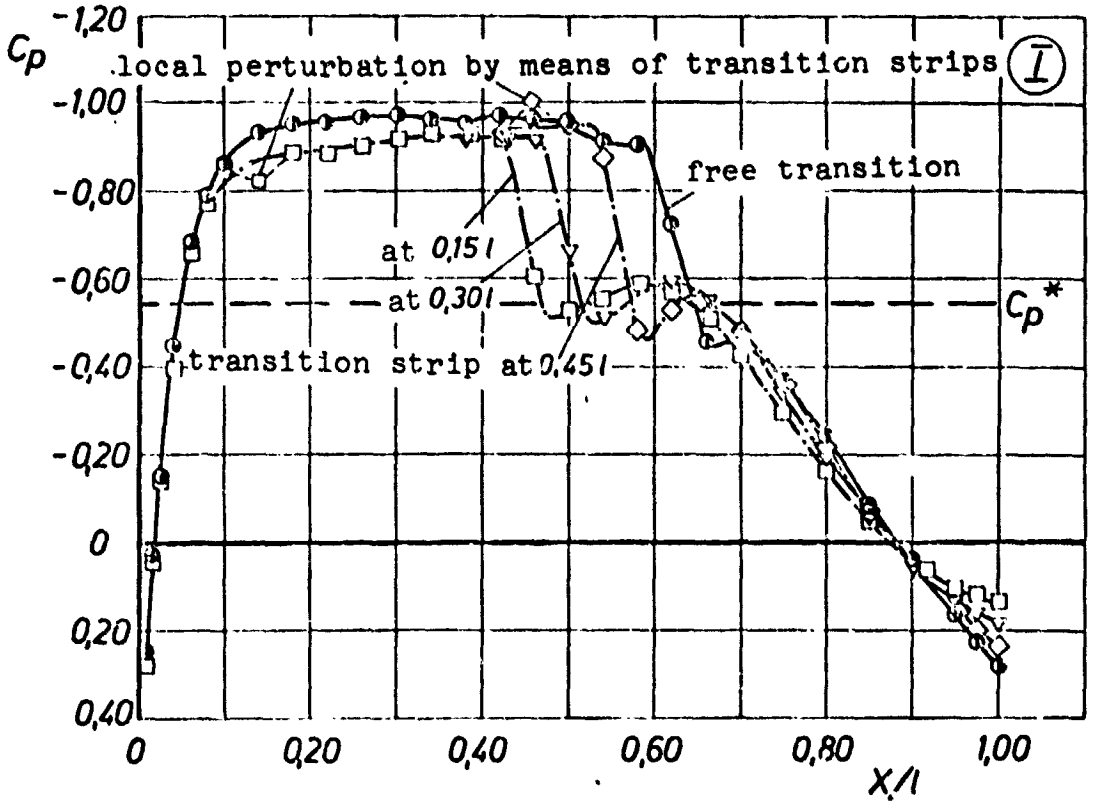

profile SF 220, CAST 10-2
$Ma = 0{,}765$; $\alpha = 2{,}0°$; $\alpha_{korr} = 1{,}3°$

Sym	Transition	$Re \cdot 10^{-6}$
◑	free	2,35
□	220 K, 15 l	2,36
▽	220 K, 30 l	2,36
◇	220 K, 45 l	2,36

FIGURE 20: Influence on the position of transition strip on the pressure distribution at $Ma = 0{,}765$ and $\alpha_{korr} = 1{,}3°$

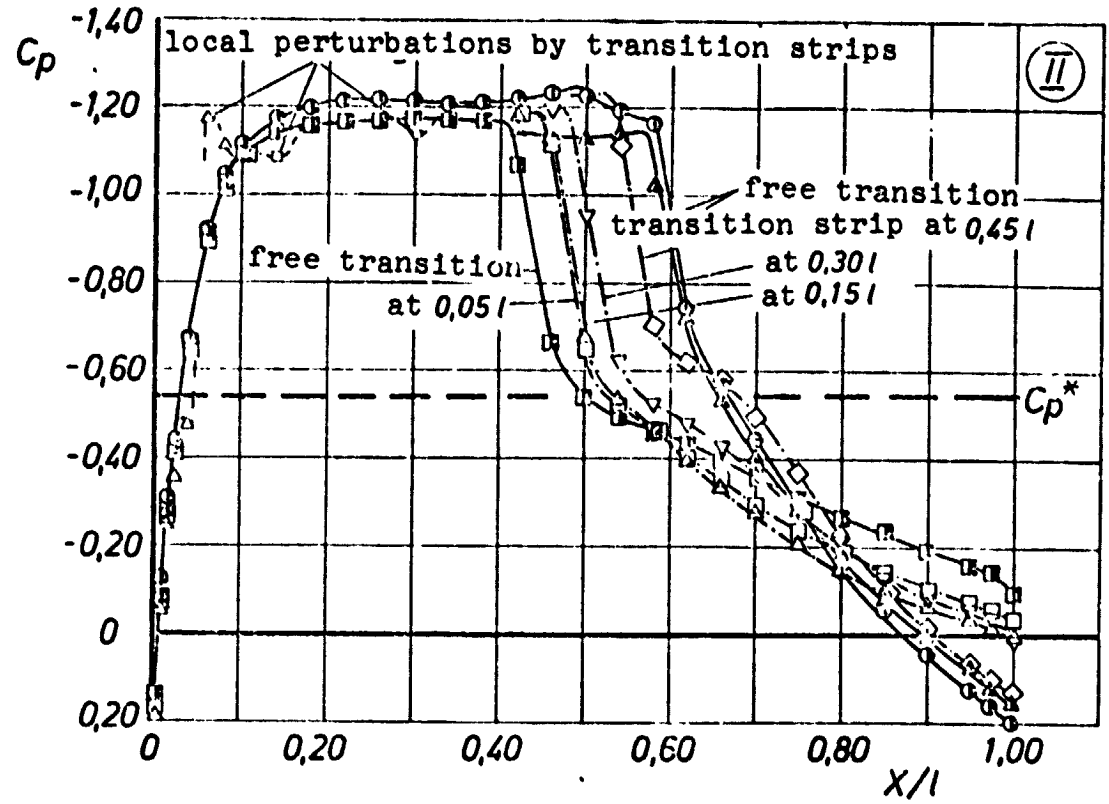

profile SP 220, CAST 10-2
Ma = 0,765; α = 4,5°; α_{korr} = 3,51°

a) suction side

Sym	Transition	Re·10⁻⁶
▲	free	1,35
●	free	2,35
■	free	3,59

Sym	Transition	Re·10⁻⁶
△	220K, 5 l	2,36
□	220K, 15 l	↓
▽	220K, 30 l	↓
◇	220K, 45 l	2,36

FIGURE 21: Influence of Reynolds number and transition on pressure distribution at $Ma = 0,765$ and $\alpha_{korr} = 3,51°$

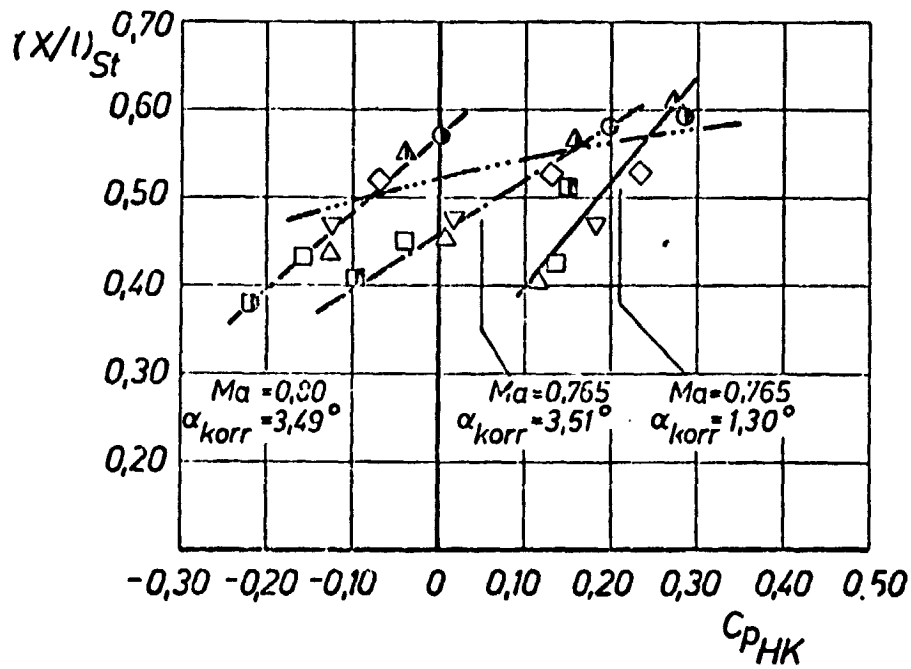

profile SP220, CAST 10-2

Sym	Transition	Re·10⁻⁶
▲	free	1,35
◑	free	2,35
◨	free	3,59

Sym	Transition	Re·10⁻⁶
△	220K, 5 l	2,36
□	220K, 15 l	↑
▽	220K, 30 l	↓
◇	220K, 45 l	2,36

—·····— relation for strong Mach number gradients ahead of shock(according to [11])

FIGURE 22: Relationship between trailing edge pressure and position of compression shock

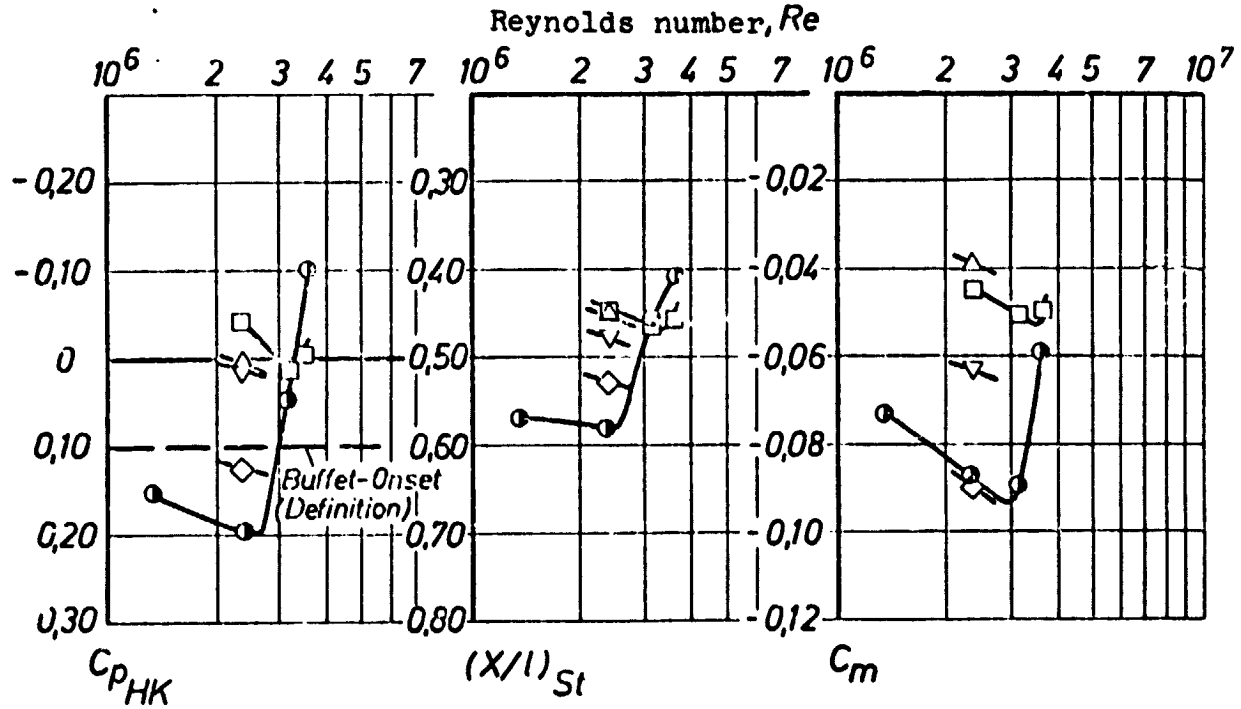

trailing edge pressure | position of compression shock (suction side) | pitch moment

profile SP 220
CAST 10-2
Ma = 0,765
α = 4,5°
α_{korr} = 3,51

Sym	Transition
◐	free
△	220K, 5 l
□	220K, 15 l
▽	220K, 30 l
◇	220K, 45 l

FIGURE 23: Influence of Reynolds number and transition on various parameters of pressure distribution

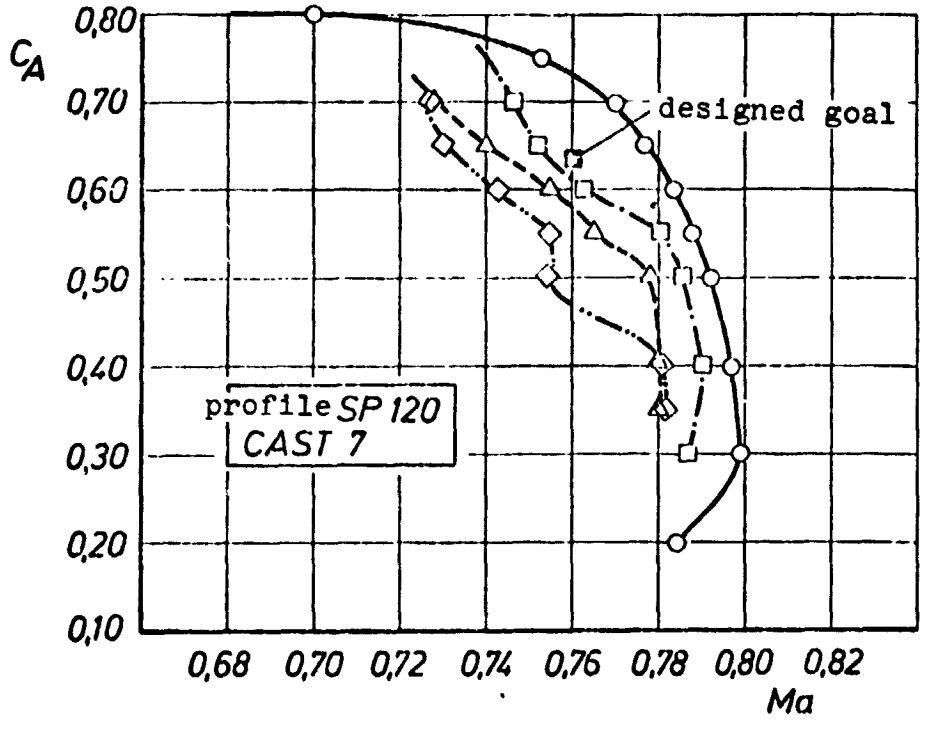

Sym	Transition	$Re \cdot 10^{-6}$
○	free	2,40
□	free	3,10
△	free	3,60
◇	220 K, 15 l	2,40

FIGURE 24: Drag rise limit for the profile CAST 7 (SP 120) as a function of Reynolds number and transition

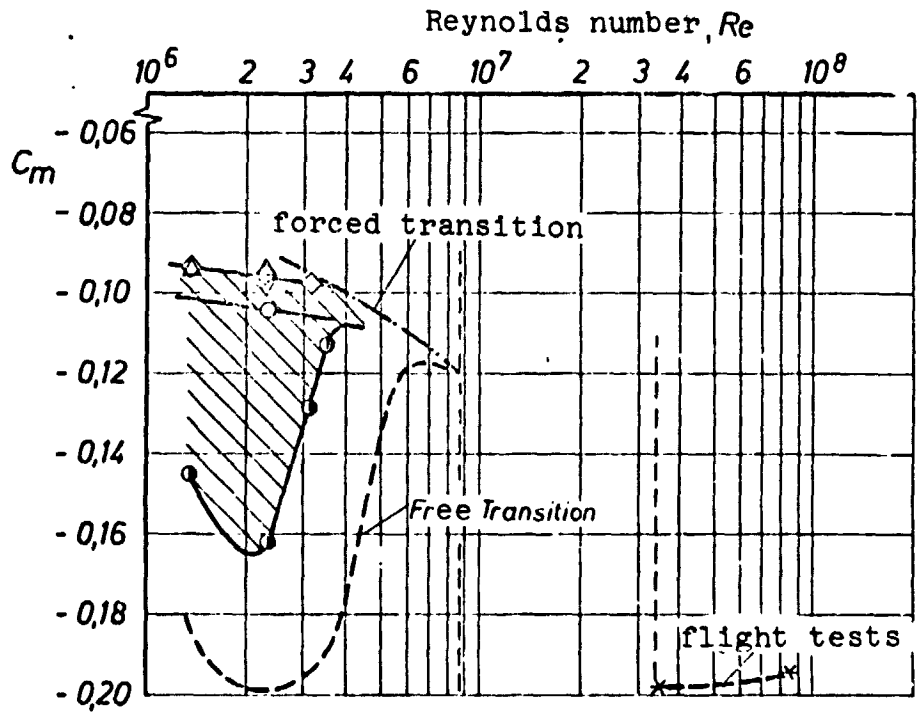

Sym	Ma	α_{kor}	config.	Transition	data source
◐	0,800	4,7°	SP 120	free	DFVLR-AVA
○	↕	↕	(CAST7)	220 K, 151	↕
▽	↕	↕	↕	220 K, 51	↕
△	↕	↕	↕	150 K, 51	↕
◇	0,800	4,7°	SP 120	100 K, 51	DFVLR-AVA
—·—	0,825	0°	C-141	7,5 l	
----	0,825	0°	η=0,389	free	[9]
*	0,825	0°	↓	"	

FIGURE 25: Pitch moment variation as a function of Reynolds number and transition for the profile and the transport aircraft C-141